Tecnológico de Costa Rica Universidad Nacional

DOCINADE
Doctorado en Ciencias Naturales para el Desarrollo

Maestría en Ciencia y Tecnología para la Sostenibilidad

Eje temático de Energía Renovable

Tesis de Maestría

Comparison of the effectiveness among different photovoltaic fault detection techniques.

Candidate

Sr. Leonardo Cardinale Villalobos

Assessor

Dr. Carlos Meza Benavidez

Tutor

Dr. Abel Méndez Porras

January 2021

TEC | Tecnológico de Costa Rica

UNA UNIVERSIDAD NACIONAL COSTA RICA

Maestría en Ciencia y Tecnología para la Sostenibilidad

Eje temático de Energía Renovable

Comparison of the effectiveness among different photovoltaic fault detection techniques

Work submitted to the Evaluation Tribunal as a requirement for applying for the degree of Master in Science and Technology for Sustainability, under the thematic axis of Renewable Energy

Evaluation Tribunal

Dr. Tomás Guzmán Hernández

AAD Coordinator, who presides

Dr. Fabián Echeverría Beirute

GMSc

Dr. Carlos Meza Benavidez

Thematic Area Coordinator

Dr. Abel Méndez Porras

Tutor

Msc. Julio Andrés Morera Hidalgo

Guest

Firmado digitalmente por TOMAS DE JESUS GUZMAN HERNANDEZ (FIRMA)
Fecha: 2021.06.07 10:39:48 -06'00'

FABIAN ECHEVERRIA BEIRUTE (FIRMA)
Firmado digitalmente por FABIAN ECHEVERRIA BEIRUTE (FIRMA)
Fecha: 2021.06.07 12:50:20 -06'00'

Firmado digitalmente por CARLOS MEZA BENAVIDES (FIRMA)
Motivo: Estoy aprobando este documento
Fecha: 2021.06.07 13:48:22 -06'00'

ABEL MENDEZ PORRAS (FIRMA)
Firmado digitalmente por ABEL MENDEZ PORRAS (FIRMA)
Fecha: 2021.06.07 14:56:58 -06'00'

JULIO ANDRES MORERA HIDALGO (FIRMA)
Firmado digitalmente por JULIO ANDRES MORERA HIDALGO (FIRMA)
Fecha: 2021.06.08 16:37:32 -06'00'

Table of contents

Declaration of authenticity

I, the undersigned, Leonardo Cardinale Villalobos, student of the Maestría en Ciencia y Tecnología para la Sostenibilidad, declare that the content of this thesis is my original work and that all the assistance received in preparing this thesis and sources have been acknowledged.

This thesis has not been submitted for any degree or other purposes and objectives of this study and has not been previously submitted to any other university for a higher degree.

Furthermore, I confirm that, I have referenced all sources used in the work and that all data and findings in the work have not been falsified or modified.

LEONARDO CARDINALE VILLALOBOS (FIRMA)

Firmado digitalmente por LEONARDO CARDINALE VILLALOBOS (FIRMA)
Fecha: 2021.06.03 22:09:35 -06'00'

Acknowledgments

Firstly, I would like to express my sincere gratitude to my tutor Dr. Abel Méndez Porras for his support and guidance in this study and related research, for his patience, motivation, and immense knowledge.

Besides my tutor, I would like to thank my assessor, Dr. Carlos Meza Benavidez for their encouragement and advice.

My sincere thanks also go to SESLab and the research group of the project "Identificación de Fallas en Instalaciones Solares Fotovoltaicas", code VIE 5402-1360-4201, for the possibility of developing the project in the photovoltaic installation they manage in San Carlos and contributing with the budget for the development of the experiment.

My special thanks to Dalberth Alberto Corrales Alpízar, John Martin Chacón Zambrana, Jose Eduardo Zúñiga Ramírez, Leninyer Gerardo Pérez Sánchez, Allán Solis González and Luis Yariel García Ramírez for their support and contribution to develop the experiments.

Dedication

I dedicate this project to God, for the gift of life and wisdom to conclude this work successfully.

To my wife Gloriana Fernández Coghi, for being my life partner during all this stage and for all the support and company during so many hours of work invested.

To my son Leandro Cardinale Fernández, who came into my life during the development of this master's degree.

To my parents Leonardo Cardinale Villagrán and Marleny Villalobos Jiménez because they formed me as a dedicated and determined person to achieve my goals.

To my family, colleagues, and friends, who accompany me in the development of each stage of my life.

Introduction.

1. Justification

Since 1990, global CO_2 emissions have increased by 50% (United Nations, 2015). Given this situation, in the Paris agreement, Costa Rica acquired the commitment of passing from 2 tons to 1.19 tons of greenhouse gas emissions per person by 2050 (Avendaño, 2017). For this reason, Costa Rica decided to carry out more research and innovation in non-conventional renewable energies (Gutiérrez Espeleta, Edgar E, 2015) identifying a potential of 576,747 MW for solar energy (Herrera Murillo, 2017).

The Instituto Tecnológico de Costa Rica (TEC), in its 2017-2020 strategic plan, establishes "Energy" as one of its main areas of knowledge, where it proposes to make more efficient use of renewable energies (Tecnológico de Costa Rica, 2017). Part of this effort is provided by the Laboratory of Electronic Systems for Sustainability of the School of Electronic Engineering at TEC (SESLab), which manages 1,200 solar panels in operation (Mata Jiménez, 2019) and this master's degree through the Doctorate in Natural Sciences for Development (DOCINADE).

Solar photovoltaic (PV) technology provides low CO_2 electricity from a free and virtually inexhaustible source (María Fernanda & Pérez-Ruiz, 2017; Miguel A & Williams, 2016). The highest performance of PV systems is determined by their lifetime (International Renewable Energy Agency, 2017), which is met when the efficiency of the system reaches 80% with respect to the initial one (International Renewable Energy Agency, 2017; Rolf Frischknecht, René Itten, Parikhit Sinha, Mariska de Wild-Scholten, Jia Zhang, 2015). The manufacturers guarantee that the efficiency of the solar modules will drop by about 0.5 % per year under normal conditions, however, PV installations are not exempt from failures, which: reduce efficiency, increase the payback time of the investment, and may cause irreversible deterioration (permanent failures) (Zhao, 2015) or even generate fires (Mellit et al., 2018). Therefore, with the growth in the number of solar farms of up to thousands of PV panels (Watson & Hudson, 2015), the search for effective fault detection strategies for PV systems has become a major issue.

There are multiple causes of failures in solar panels that are being studied to find solutions. Maghami (2016) studied the effect of soiling, Mekki (2016) analyzed partial shadows, and Zhao (2015) the electrical failures. Besides them, many other research works have been written about these faults, because they are among the most common (Madeti & Singh, 2017).

To counteract this problem, multiple alternatives for failure detection have been developed. However, despite great efforts to generate better methods for failure detection, more experimental research is lacking in real low-cost systems (Mellit et al., 2018) and insufficient information has been detected to quantitatively compare different detection techniques.

The need to compare the existing alternatives in failure detection techniques has caused the generation of scientific research around the topic, for example, the authors Appiah, Zhang, Ayawli, & Kyeremeh (2019) have made a comparative analysis from the review of 40 articles, in which, it was identified that no quantitative data is detailed, such as the accuracy of the techniques.

The authors Mellit, Tina, & Kalogirou (2018), from a literature review, identified the advantages and limitations of multiple techniques for detecting, locating, and classifying faults in PV arrays. This study highlights infrared thermography (IRT) and visual inspection (VI) techniques, mentioning that they are suitable for small and large scale installations. Also, Tsanakas, Ha, & Claudia Buerhop (2016) recommend their use by drones to speed up the work. Concerning electrical analysis (EA) techniques, Mellit, Tina & Kalogirou (2018) y Ventura & Tina, (2016) highlight that they have low hardware requirements, can detect practically any failure in the array, and apply to small and large scale installations.

Therefore, according to Appiah (2019), Mellit (2018), Tsanakas (2016) and Ventura (2016) the current challenges were identified as: a) to implement economically profitable techniques, b) to develop efficient techniques, easy to implement, scalable to different technologies and small-scale installations, which classify, identify and detect new failures. They recommend, a) experimenting in low-cost electronic solutions that transmit information over the Internet, b) integrating at a large scale the methods designed with experimental validation to analyze the cost-complexity relationship.

Considering that: a) there is a theoretical frame of reference about the failures and existing methods to detect them, b) there is a need to carry out experimentation in this subject through real cases, c) there is a lack of studies of quantitative experimental comparison between methods and d) the techniques of VI, IRT, and EA (by efficiency analysis), with low-cost platforms, are techniques that have a high potential. Therefore, the following research question was identified: What is the most effective method of detecting failures in solar panels? To contribute to answering the previous question, the scope of this research was defined as: to compare the effectiveness of IRT, VI, and EA from a quantitative and experimental approach, inducing failures due to soiling, shading, and electrical faults. As mentioned, the answer to this question will contribute to Sustainable Development and make PV generation more profitable by providing information that will be used to increase the lifetime of PV systems.

2. Theoretical framework

2.1. Renewable energies in the context of sustainable development

With the 1987 report called “Our Common Future” by the World Commission on Environment and Development, the term "Sustainable Development" became more important. Sustainable development can be understood as: "meeting the needs of the present generation without compromising the ability of future generations to meet their own needs" (Asamblea General de las Naciones Unidas, 2019). With the increase in society's needs, the challenge of meeting them sustainably over time has arisen.

Goal 7 of the Millennium Development Goals for Sustainable Development states "Ensure environmental sustainability". Society's energy demands are constantly growing, such is the case of the United States, wherein 2018 energy consumption was the highest in history (McFarland, 2019). Given this reality, renewable energies have a fundamental role to play, since they contribute to sustainable development in the fight against climate change. Thanks to the best technologies, competitiveness, and international experience developed, renewable energies have decreased their cost, making some projects even more profitable than fossil fuel generation (International Renewable Energy Agency, 2017).

2.2. Description of PV systems

PV generation systems represent one of the most promising forms of renewable energy transformation today, as their cost has decreased by 80% by 2017 with respect to 2010 (International Renewable Energy Agency, 2017). They allow transforming the energy contained in solar radiation into electric energy employing solar cells. The increase in the use of these systems has made it possible to generate greater technical-scientific knowledge and achieve greater efficiencies over the years (International Renewable Energy Agency, 2017). At present, manufacturers of solar panels guarantee a lifetime between 25 and 30 years (International Renewable Energy Agency, 2017; Rolf Frischknecht, René Itten, Parikhit Sinha, Mariska de Wild-Scholten, Jia Zhang, 2015), at a time they operate at 80% efficiency, however, they continue to operate normally after this period.

PV systems that are connected to the grid are made up of the following components: 1) solar panels, 2) inverter, 3) breaker panel, 4) power meter, 5) utility service, and 6) consumer loads. In this type of system, the inverter seeks to extract as much energy as possible from the solar panels, which is delivered to the load, and the excess is delivered to the grid (ACESOLAR, 2019). A general diagram of the parts of a grid-connected PV system is shown in Fig. 1. In this document, attention is paid to the solar panels, which correspond to an arrangement of cells that are electrically interconnected with each other. The solar panels are connected in series or parallel arrays to the inverters (see Fig. 2).

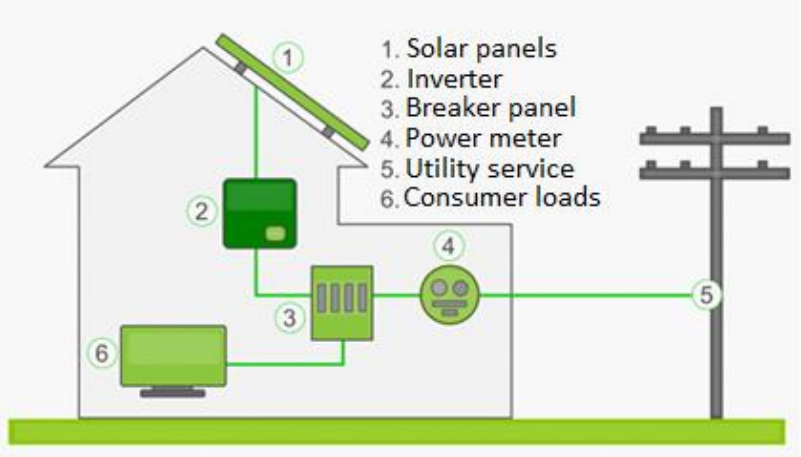

Fig. 1. Main components of a grid-connected PV system. The inverter converts direct current into alternating current, leaving the panels connected to the grid so that they can work at maximum efficiency (ACESOLAR, 2019).

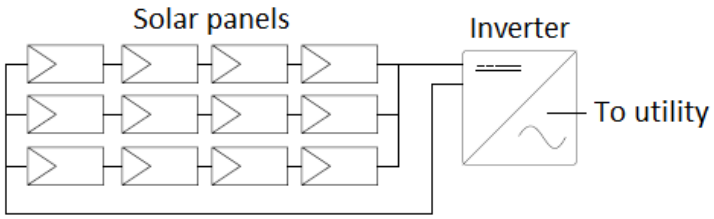

Fig. 2. PV installation configuration constituted by 3 parallel strings of 4 panels in series each.

2.3. **Solar panel failures**

Each of the components that are part of the PV system is susceptible to failure (Kazem & Jabar H, 2016), these failures will affect the operation of the system, which may decrease the performance temporarily or permanently, which consequently implies a decrease in its lifetime (Madeti & Singh, 2017). Among the parts of a PV installation, solar panels are the energy-generating component, therefore, a failure in this one will have a direct impact on the system performance, hence the priority that has been identified in finding failures in this component before others (Gallardo-Saavedra, S., Hernández-Callejo, L., & Duque-Pérez, 2019).

Some of the failures that can be found in solar panels are partial shading, soiling, and electrical faults (Chine et al., 2016; Mellit et al., 2018; Murillo-Soto & Meza, 2020a). Each of these is described below:

A. Soiling failures

The soiling of PV panels causes a reduction of the generated power, which is considered a temporary failure (Livera et al., 2019). Dirt, dust, leaves, pollen, or grasses are examples of substances that cause

soiling of solar panels, the reduction in PV module performance is greater as the soiling increases (Maghami et al., 2016).

Soiling due to dust consists of particles of different sizes and materials that cover the entire photovoltaic module, which eventually forms uniform layers of dust and regions with greater accumulation of soiling (Javed et al., 2017).

Soiling due to leaves, bird drops, or patches of dirt, covering only a few cells of the PV module, generates non-uniform soiling. This has a severe power loss effect and is associated with both soiling and partial shading. PV cells that capture less irradiance will have a lower short circuit current than the rest, forcing the entire module to decrease its generated current and causing a hot spot to appear (Maghami et al., 2016). Fig. 3 shows a dirty solar panel that accumulated natural dirt distributed in non-uniform patches.

Fig. 3. Monocrystalline PV module used in this research for the evaluation of natural soiling. It is possible to observe the presence of non-uniform dirt.

B. Partial shading failures

In a string of solar panels in series, if one of the panels is exposed to partial shading, the power generated will decrease and this decrease will depend on the portion of the module that is shaded and the degree to which it is shaded (Maghami et al., 2016; Mäki & Valkealahti, 2012). The degree of shading depends on the decrease in irradiance that affects the PV module. It can be weak when the irradiance decreases a little or strong when the irradiance decreases a lot in the shaded area. Also, it has been found that under strong shading conditions the power falls linearly as the shaded area increases, and under a high percentage of shaded area conditions, the power falls linearly as the degree of shading increases (Mäki & Valkealahti, 2012). An example of weak and strong shading can be seen in Fig. 4.a and Fig. 4.b, respectively.

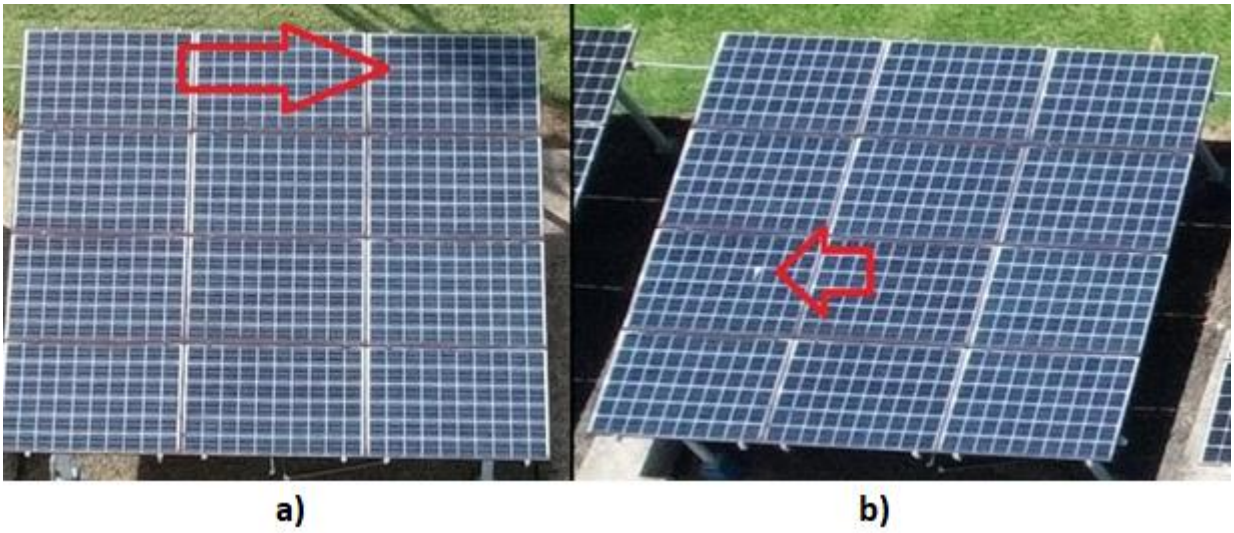

Fig. 4. Solar panels with partial shading. In Fig 4.a a weak partial shadow is identified due to a tree that interrupted the passage of direct radiation. Figure 4.b shows a strong shading due to a foreign object on the panel.

C. Electrical faults in the solar panels

From the electrical point of view, the failures can be classified as follows, 1) ground faults, 2) faults between nodes, 3) open circuit faults, 4) others (Zhao, 2015). Faults cause a decrease in the power delivered and an increase in the temperature that varies according to the type of fault (Appiah et al., 2019; Chaudhary & and D.K. Chaturvedi, 2018; Tsanakas et al., 2016; Yadong Wang et al., 2016). The types of failures studied in this research are illustrated in Fig. 5.

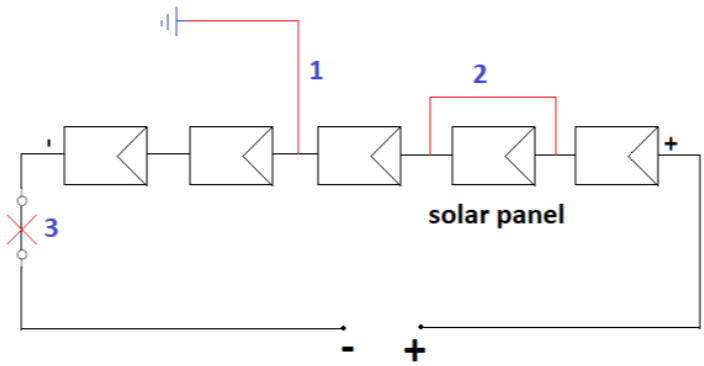

Fig. 5. Types of solar cell failures. 1) Short circuit to ground, 2) short circuit in a panel and 3) open circuit.

2.4. Failure detection methods for solar panels

Given the importance of diagnosing faults in solar panels, different techniques have been developed for this purpose. Each technique has different characteristics, for example, cost, possible failures to be detected, the complexity of the application, among others (Chen, Y H, Liang, R, Tian, Y, Wang, 2016). VI

is the first method to be used because it can be done without specialized equipment (Grimaccia, F, Aghaei, M, Mussetta, M, Leva, S, Bellezza Quater, 2015; Madeti & Singh, 2017). EA is highly implemented as the installation records the main variables (Ali, Mohammed Hassan, Rabhi, Abdelhamid, Hajjaji, Ahmed El, Tina, 2016; Chen, Y H, Liang, R, Tian, Y, Wang, 2016; Nemet, Gregory F, O'Shaughnessy, Eric, Wiser, Ryan, Darghouth, 2017). IRT is increasingly being used on a commercial basis (Alsafasfeh et al., 2017; Palmer Wahl Instrumentation group, 2007). Each has different capabilities and limitations for fault detection, among them, VI, IRT, and EA are classified as "advanced detection and diagnostic methods" (FDD) (Appiah et al., 2019; Madeti & Singh, 2017; Mellit et al., 2018). Techniques for analyzing electrical variables are subclassified into, (a) comparison, (b) statistical and signal processing-based, (c) reflectometry-based, (d) machine-learning-based, and (d) other techniques (Appiah et al., 2019; Madeti & Singh, 2017; Mellit et al., 2018). The techniques mentioned are briefly described below.

a) Detection of faults by VI

It consists of periodically observing visually the general state of the solar cells (Madeti & Singh, 2017). This method takes as a reference state the visual appearance of the solar panels in optimal conditions and compares it with the current visual condition of the solar cells. The visual differences are evaluated and interpreted to identify if they correspond to a failure and if possible to identify the type of failure (National renewable energy laboratory, 2012).

The method can be done with a camera or personally by an inspector. For the correct application, it is required to use the light conditions according to the IEC61215 standard, also, it must be done at different angles to eliminate errors due to reflection. For more information related to the maintenance of solar cells by visual inspection, please refer to the reference (Haney & Burstein, 2013). Fig. 3 and Fig. 4 are examples of suboptimal conditions that can be visually detected.

b) Fault detection by infrared thermography

This method uses the pattern of heat radiated by objects in the infrared spectrum (Land Instruments International, 2004), which cannot be seen by the eye but can be seen by a thermal camera. Objects with some damage vary their thermal image, being possible to detect them with infrared thermography. The heat pattern of solar cells can be analyzed with thermal cameras (Kaplani, 2012).

Under normal conditions all solar cells in a station will be exposed to the same solar radiation, generating the same power. Electrical conduction generates heat in the cells so that they all have the same thermal image. With the existence of short-circuited cells, false electrical contact, cell resistive problems, partial shadows, among others, there will be a higher temperature with respect to the faultless cells (Moretón et al., 2015). Any problem that generates temperature increase in the faulty cells will be visible as hot spots in the thermal image, that is, the infrared thermography method is based on the comparison of thermal

images between elements in good conditions and elements that are not. For example, in Fig. 6 it is detected from a qualitative analysis that a solar cell is hotter than the rest and in Fig. 7 a panel is observed that has certain sections that are hotter in comparison with the neighboring panels.

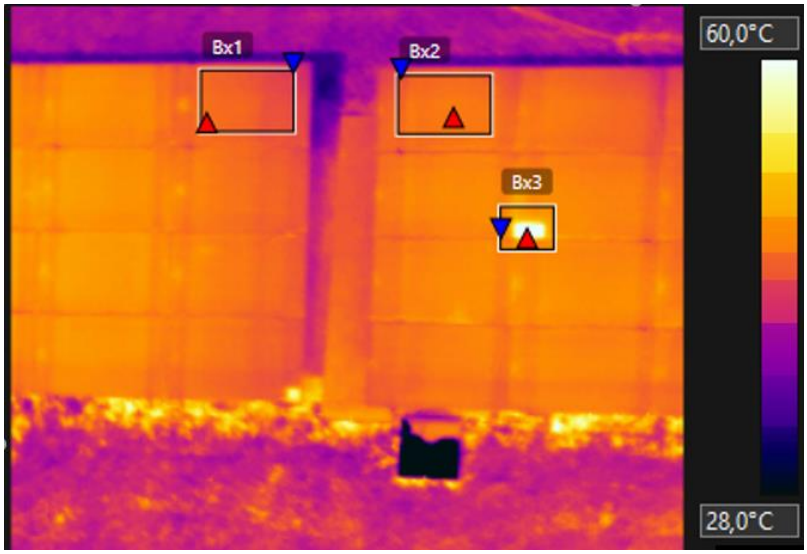

Fig. 6. Thermal image of PV arrays taken at a height of 25 m with a Flir Vue Pro R camera. In this thermogram, dark colors represent lower temperature and light colors represent higher temperature.

IRT uses the measurement of energy by infrared radiation and automatically estimates the temperature of the object. However, for the calculated temperature to be correct, it is required to make a detailed analysis of the object of interest using specialized software, for which it is necessary to know: the emissivity of the object, the distance between the camera and the object, the reflected temperature and the relative humidity (Land Instruments International, 2004). As an example, it is possible to know quantitatively the temperature differences that are observed in Fig. 6 and Fig. 7.

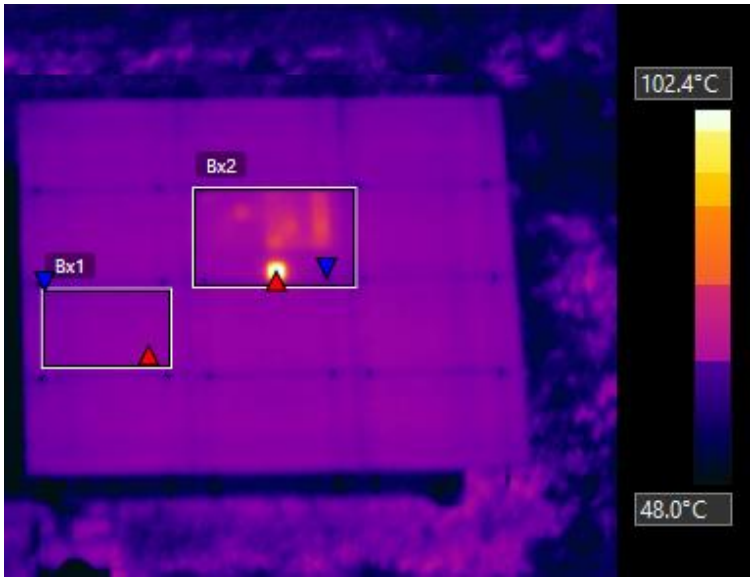

Fig. 7. Thermal image captured in this investigation of a PV array with a hot spot due to a short circuit in the panel that is observed to be hotter.

c) Fault detection through EA

Multiple techniques use analysis of electrical variables for fault detection, including statistical methods through signal processing (Zhao, 2015), current-voltage curve analysis (I-V) (Mellit et al., 2015), power loss analysis (Chen, Y H, Liang, R, Tian, Y, Wang, 2016) and through voltage and current measurements (Jones et al., 2016). These methods are based on the analysis of the electrical model of the solar panels.

The main variables that determine the power delivered by a PV array are the irradiance and temperature of the cells, therefore, knowing these variables and the characteristics of the PV array it is possible to estimate the generation of the cell (Evans, 1981). Murillo-Soto & Meza (2020b) proposed a method based on the comparison of the generated power with the theoretical power by estimating the instantaneous efficiency. The method uses the mathematical model shown in equation (1).

$$\eta_T(T, G) = (K_1 T + K_2 G + K_3) \quad (1)$$

Where K_1, K_2 y K_3 are determined by equation (2) from the solar panel manufacturer's data.

$$K_1 = (b_3 c_2 - b_2 c_3)/a_2 b_3,\ K_2 = c_2/b_3\ ,\ K_3 = (\eta_{stc} - T_{stc} K_1 - G_{stc} K_2) \quad (2)$$

Where, $a_2 = T_{noct} - T_{stc}$, $b_2 = G_{noct} - G_{stc}$, $c_3 = \eta_{pli} - \eta_{stc}$. *Stc, noct,* and *pli* are the standard conditions, conditions under nominal temperature, and performance under low irradiance conditions, respectively.

The model shown in (2) corresponds to the power generated at the terminals of the PV array, therefore, for greater accuracy the actual conditions should be considered, e.g., wiring losses and aging losses (Murillo-Soto & Meza, 2020b).

3. Objectives

3.1. General objective

Compare the effectivity of failure detection techniques based on visual inspection, infrared thermography, and measurement of electrical variables through a case study on solar panels with specific failures to contribute to the state of photovoltaic installations.

3.2. Specific objectives

1. To design a protocol for the quantitative evaluation of the effectivity of failure detection techniques in solar panels of interest for conditions of soiling, partial shading, and electrical faults.
2. To develop an experiment that evaluates each of the failure detection techniques in PV strings in operation under defined conditions of soiling, partial shading, and electrical failures for the generation of quantitative indicators of effectivity.
3. To compare the effectivity of each technique through descriptive and inferential statistics for the determination of the capacities and limitations of each technique in failure detection.

4. **Methodological framework**

The project was developed through a case study with a quantitative approach and descriptive scope applying an experiment. According to Hernández Sampieri (2010) and Wohlin (2012), a case study is appropriate for this research because it has the following characteristics:

a) can be used in complex, unpredictable, and dynamic environments, under conditions where you do not have control of all variables.
b) works for comparative research between methods.
c) can generate qualitative or quantitative conclusions from multiple sources of information.

It was defined as five general and systematized stages as established by Wohlin (2012) for a case study. The stages were:

1) Design and planning (objective 1): Based on the objectives and the defined research question, the object of study was identified, a theoretical framework, the methods for the collection of information, and the sample for the experiment were collected.
2) Protocols (objective 1): Procedures to apply each failure detection method and the criteria for the detection of the failures of interest were established.
3) Preparation and data collection (objective 2): An experiment was applied under real conditions of minimum control as established by Hernández Sampieri (2010).
4) Data analysis (objective 3): Quantitative analysis of the information collected with its respective validation.
5) Results report (objective 3): Generation of research conclusions.

The following describes each of the stages.

4.1. **Design and planning (objective 1)**

A) Literature Review

The project began by reviewing the literature, which identified the current problems and established a solution that met the objectives of the research. The following is the procedure followed for the literature review:

A search of scientific articles was performed in the Web of Science database. Keywords were used which were then combined with logical AND or OR operators as required. The search included: 1) photovoltaic systems, 2) failure detection methods, 3) visual inspection, 4) electrical analysis, 5) infrared thermography. Each search also included similar terms (synonyms) to find a larger number of articles; the results were limited to the last 5 years. The search yielded 158,400 articles with the first filter and then ended with 130 articles when all filters were applied. Then, sorting by relevance was applied and the 11 articles with the

greatest relation to the topic and the greatest number of citations were selected. Finally, the 5 articles that were identified as most related to the topic of interest were selected to establish a current framework.

Subsequently, to expand the conceptual framework, scientific articles with less than 10 years of publication, books, standards, and technical notes from equipment manufacturers and service providers related to the subject that show current information were studied.

B) Population and data collection methods

With the recognition of the problem, solar panels were identified as the object of study, since they have a significant effect on the performance of the system in comparison with the other components of a photovoltaic installation (Gallardo-Saavedra, S., Hernández-Callejo, L., & Duque-Pérez, 2019).

Other case studies related to the experimental failure analysis in photovoltaic systems, which used one or more of the methods of this project, were taken into account to select the population and the methods of information collection.

4.2. **Protocols (objective 1)**

The protocols for the development of the experiment considered the following aspects:

a) Procedures required for each technique to be considered valid.

Each one of the techniques is different, therefore, through a bibliographic review, the conditions required for the application of each one were established, which were also focused on the detection of the failures of interest.

b) Criteria for the detection of each failure.

A bibliographic review was made that established the characteristics of the information given by each technique in case any of the study failures were detected. This criterion allowed generating a binary response signal of the form: detected or not detected.

4.3. **Preparation and data collection (Objective 2)**

A second-degree data collection was implemented, i.e., it was done at the time, but without direct contact with the object (Wohlin et al., 2012), this considering that all tests do not have a permanent effect on the PV modules. Also, each measurement was made using pre-test conditions to indirectly control the variables of the experiment (Hernández Sampieri et al., 2010), for this, the time and climate conditions required were planned according to the protocols.

The measurements were made by category 4 observation, i.e., with a low level of interaction by the researcher and the object is not aware of being observed (Wohlin et al., 2012). The information was

digitally archived to achieve dependence on the reliability of the research (Hernández Sampieri et al., 2010).

4.4. **Description of the instrumentation used during the experiment (objective 2)**

From the protocols and nature of each technique under study, the requirements of the instrumentation for data collection were identified.

4.5. **Design of the experiment (objective 2)**

The available resources and the nature of the study implies having to work with a small sample, so a design of repeated measurements by replication was used (Tango, 2017); in this study, two PV arrays were tested as study subjects. Each array was treated for each type of failure studied and evaluated using all three techniques. A control subject was also available to validate that each treatment corresponded to a real failure.

4.6. **Data analysis (objective 3)**

The data were interpreted from statistical analysis with a comparative approach of the effectivity of each studied technique. Data analysis was done with Jamovi 1.1.9.0 statistical software, starting with descriptive statistics through an exploratory analysis of the data and then inferential statistics through contingency tables with hypothesis testing (Hernández Sampieri et al., 2010).

4.7. **Report of results (objective 3)**

Conclusions were generated that were reflected in three scientific articles and this master's thesis.

Synthesis.

1. Summary of the thesis

The main objective of this research was the quantitative comparison of the effectivity of three failure detection techniques in PV systems: a) VI, b) IRT, and c) EA; focused on the detection of partial shadows, soiling, and electrical failures. For this, an experiment was developed in a PV installation at the San Carlos Local Technological Campus of the Tecnológico de Costa Rica. The VI and IRT techniques were made using an unmanned aerial system and the electrical analysis compared the generated power with the estimated power using an embedded system Raspberry Pi 3 model b; each technique was implemented using low-cost instrumentation. The results showed that there were no significant differences in the total amount of failures detected by the three techniques; however, the VI was the best at detecting soiling and the worst at detecting electrical failures. Also, partial shadows were the type of failure that was most detected by all the techniques. Therefore, to detect as many faults as possible, VI should be combined with IRT or EA. This research contributes to the search for better fault detection techniques, also, the methodology developed can be replicated to compare other techniques and other types of faults. Finally, the results create objective indicators for the generation of suitable maintenance plans that will achieve a greater contribution to the environment and more profitable generation projects.

2. Articles

The thesis was developed from a compendium of three articles, as indicated below:

1. Cardinale-Villalobos, L., Rimolo-Donadio, R., & Meza, C. (2020). Solar panel failure detection by infrared UAS digital photogrammetry: a case study. International Journal of Renewable Energy Research (IJRER), 10(3). https://ijrer.com/index.php/ijrer/article/view/1104*Indexed in Scopus*

2. Cardinale-Villalobos, L., Meza, C., & Murillo-Soto, L. (2020). Experimental comparison of visual inspection and infrared thermography for the detection of soling and partial shading in photovoltaic arrays. In S. Nesmachnow & L. Hernández Callejo (Eds.), Smart Cities, Third Ibero-American Congress, ICSC-Cities 2020, San José, Costa Rica, November 9-11, 2020, Revised Selected Papers (1st ed.). Springer International Publishing. https://doi.org/10.1007/978-3-030-69136-3 *Indexed in Scopus*

3. Cardinale-Villalobos, L., Meza, C., Méndez-Porras, A. & Murillo-Soto, L. D (2021). Quantitative comparison of infrared thermography, visual inspection, and electrical analysis techniques on

photovoltaic panels: a case study. *To be submitted*.

Each one of the articles has a contribution to the specific objectives of the thesis, allowing this, to reach the general objective of the research. The contribution of each one is indicated below.

The protocols (**objective 1**) of each technique studied were determined from the review of the literature. In article 1, the IRT is presented in detail and the protocol is tested in an experimental approach. The protocol of the VI is presented in article 2 and for the EA in article 3.

Article 2 presents the design of the research experiment (**objective 2**) and it is used to compare IRT and VI in the presence of soiling and partial shading faults.

Article 3 develops **objective 3**. In this one, the design of the experiment of article 2 was replicated, now to compare the effectivity of the three techniques (IRT, VI, and EA) considering the three faults of interest (partial shadows, soiling, and electrical faults).

Article 1.

Solar panel failure detection by infrared UAS digital photogrammetry: a case study.

Journal: International Journal of Renewable Energy Research

Authors: Cardinale-Villalobos, L., Rimolo-Donadio, R., & Meza, C

Year: 2020

Volume: 10

Number: 3

Indexed in Scopus

Solar panel failure detection by infrared UAS digital photogrammetry: a case study.

Leonardo Cardinale-Villalobos *‡, Renato Rimolo-Donadio **, Carlos Meza**

*Department of Electronic Engineering, Instituto Tecnológico de Costa Rica, Santa Clara, Alajuela, Costa Rica

**Department of Electronic Engineering, Instituto Tecnológico de Costa Rica, 30101 Cartago, Costa Rica

(lcardinale@tec.ac.cr, rrimolo@tec.ac.cr, cmeza@tec.ac.cr)

‡ Corresponding Author; Leonardo Cardinale Villalobos, Santa Clara, Alajuela, Costa Rica, Tel: +506 2401 3021

lcardinale@itcr.ac.cr

Received: 11.06.2020 Accepted:13.07.2020

Abstract- Infrared thermal photogrammetry is an attractive solution for the diagnosis of photovoltaic systems. Traditional systems often require high-end drones and expensive cameras, but more recently, low-cost thermal sensors on board of small-scale drone platforms suitable for digital photogrammetry have emerged as a promising approach. Nevertheless, studies evaluating its effectiveness can barely be found in the literature.

Unlike many works in the literature that analyze individual images, through digital photogrammetry it is also possible to create orthomosaics of complete installations or high-resolution maps of segments that cannot be visualized and analyzed properly with single images.

In this work, a photogrammetric thermal analysis methodology with a small-scale drone and a thermal camera is presented and a case of study is analyzed. To validate and quantitatively scale the results, functional tests on the panels were performed and temperature measurements with a thermocouple on the panels were carried out. The results from both single images and orthomosaics confirm that it is possible to obtain qualitative and quantitative information to detect failures in solar panel installations with a low-cost thermal sensor on board of small-scale drone platforms. These results may be useful for defining surveillance and maintenance procedures with low-cost equipment in photovoltaic installations, which can help for early detection of failures, operation with higher efficiency and to achieve longer lifetimes of the panels.

Keywords Photovoltaic system, Photogrammetric techniques, Infrared thermal imaging, Unmanned aerial vehicle, Solar panel.

1. Introduction

Steady cost reduction in photovoltaic (PV) solar technology has made it possible to significantly increase the number of installations worldwide. PV installations with hundreds of thousands of PV modules that occupy thousands of hectares are not uncommon [1]. In grid-connected solar installations, PV modules are connected in series, forming strings that are then connected in parallel. In this scenario, a fault in a single cell in a PV module affects all the modules electrically connected to it.

In this context, techniques related to the operation and maintenance of PV modules acquired greater importance. As reported in [2], expert visual inspection and fault analysis in a 3 MW installation take 60 days. Thus, developing techniques that diagnosticate faults efficiently in shorter times becomes a necessity.

Multiple failures can manifest in solar modules, some of them are shading and hot spots [3, 4, 5]. Shading exists when there are cells of a solar panel that are subjected to less solar radiation due to external shadows (see Fig. 1) [6, 7, 8, 9, 10]. Hot spots exist when at least one solar cell in an illuminated module has a considerably smaller short-circuit current than the other cells [11]. All of the above-mentioned faults cause an efficiency decrease [12, 5, 13, 14], i.e., they correspond to sub-optimal operating conditions.

Fig. 1. Example of a solar panel with a partial shadow.

Infrared thermography (IT) is a failure detection technique [15], which is based on the analysis of thermal images of solar panels [16, 17], it allows the identification of temperature gradients or hot spots that can be associated with panel failures [16, 18, 19]. This failure detection technique does not require contact with the element of interest and generates a large amount of qualitative and quantitative information for each image; this allows the estimation of the temperature of each pixel in the thermogram [11]. Fig. 2 shows a fault detected in a solar panel by a thermogram taken with a drone.

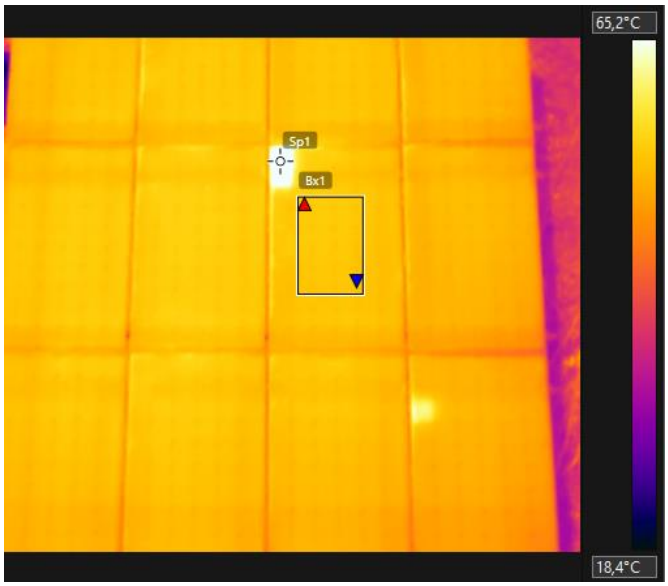

Fig. 2. Solar panel thermogram showing a fault (hot spot), taken with a drone.

The correct application of IT can be complex, especially in the large areas of solar farms with thousands of PV panels. Because the solar panels are oriented upwards and sometimes on roofs, it is often necessary to make the inspections from high points. Unmanned aerial systems (UAS), also known as drones, with onboard thermal cameras, are therefore a useful tool for this task; they enable inspections from the air and through digital photogrammetry techniques it is possible to detect failures in an agile way [11, 20]. Fig. 2 shows an example of a thermogram taken with a drone.

Due to the variety of failures and a large number of solar panels that can be involved in an inspection, the capabilities of the drones and the requirements for IT analysis demand a systematic engineering planning for each mission that include both photogrammetry and individual thermograms [21, 11].

This article demonstrates that it is possible to detect failures in solar panels with low-cost drones and thermal cameras, both through individual image and orthomosaic analysis, applying procedures similar to those available in the literature that had been validated with high-end equipment. This work provides an approach that might contribute making decisions in the maintenance management of photovoltaic systems.

The article is structured as follows: Section 2 discusses briefly previous works and the tools and methods applied, section 3 addresses the configuration of the experiment, and section 4 shows the results with their respective analysis. Section 5 gathers the main conclusions and perspectives for further work.

2. Photovoltaic fault detection and infrared thermal photogrammetry

Two main aspects of fault detection are considered in this work: the presence of hot spots and partial shading. After discussing briefly both cases, the basics for their assessment through UAS imagery and photogrammetry are discussed in this section.

2.1. Thermal imaging characterization of solar panels with hot spots

In a solar panel, multiple failures manifest as hot spots, i.e., small surfaces in a PV cell that exhibit an anomalously high temperature with respect to the neighbouring areas. For example, in [22], the following thermal gradients have been related with faults: a) poor thermal conductivity of the cell's encapsulation material reached 100 °C, b) a micro defect in the cell reached 71.3 °C and c) deformations in resins with a temperature of 136.1 °C. In [11], hot spots were detected due to: cell breaks, false contacts, defective welds, and inactive modules due to bypass diode failures [11].

A hot spot varies in size depending on the type of fault, for example, we can find faults that cover a set of cells (open circuit [11]) or a fraction of the cell (microdefect [22]). Thus, the size of the fault is a parameter that determines the spatial resolution required for the images taken in a drone mission, a parameter known as ground sampling distance (GSD). The temperature variation due to a hot spot is also an indicator of the severity of the fault, where less than 10° is considered within the normal operation tolerance [23, 15]; however, at lower irradiance, the temperature variation of a fault will decrease [24].

2.2. *Characterization of panel thermograms with partial shading*

The region of a solar panel that is found to have lower radiation levels, i.e., it is partially shaded, will experience a higher temperature [21, 25]. This type of hot spot can range from a fraction of a cell (e.g., bird droppings) [11] to multiple cells (e.g., the shadow of an object close to the panel) [21]. According to tests carried out by [26, 27], there may also be cases in which a shadow that covers several cells of the panel, not all or only one, will experience heating. The temperature variation in tests made by [27] with partial shadows was between 10 °C - 20 °C, however, smaller temperature variations were also found.

2.3. *Digital photogrammetry*

Panel faults can be of different sizes and must be detected most of the time over large installations, which imply that a large number of images with good resolution are required. Since from many single images it might be difficult to identify the exact position of the fault, digital photogrammetric techniques can be used for the creation of orthomosaic views of the complete area with georeferencing, thermogram raster and three-dimensional (3D) or 2.5 D profiles of the installation from a set of 2D images.

To apply this technique, images should be taken along a predefined flight route that covers the area under study and provides enough lateral and frontal overlap among images (of at least 60%). The data set is then processed to find coincidence points among images in order to align them, as depicted in Fig. 3. From this step, the matched points are used to project the model in a 3D space in the form of a sparse point cloud. This cloud is refined to create the dense point cloud from which diverse photogrammetric products such as orthomosaics or digital elevation models.

The flow used in this work is based on the well know SIFT and SfM algorithms, implemented in the commercial software tool called Agisoft Metashape, which is the same described in [28, 29].

2.4. *Considerations for implementing photogrammetric surveys*

In our approach, it is assumed that the thermal camera uses an uncooled microbolometer sensor (UMS) that measures infrared radiation and thus estimates the temperature of the object [21]. This means that the camera does not perform a direct measurement of temperature and therefore the acquired images require interpretation.

The measurement should be made at a time with sufficient irradiance to allow the capture of thermal contrasts, with a correct angle and without wind currents that generate convection cooling [21], constant sunlight conditions with a clear sky are also desirable so that solar panels in good conditions have a homogeneous thermal distribution [11]. In [21], it is recommended to have an irradiance between 500 W/m^2 and 700 W/m^2 and to capture the images with an angle between 5° and 60° with respect to the perpendicular of the

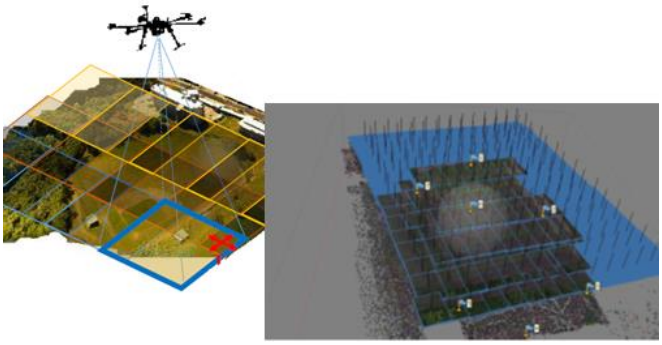

Fig. 3. Illustration of a photogrammetric survey and aligned post-processed images to construct the point clouds.

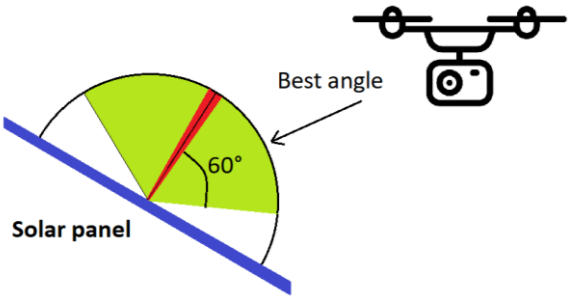

Fig. 4. Recommended orientation of the thermal camera with respect to the panel position.

panel (see Fig. 4). In [15] they indicate that the irradiance should be greater than 700 W/m^2 with an angle between 0° - 30° from the perpendicular direction. Also, the drone can create a partial shadow, so it is recommended to take the measurements in the morning or the afternoon, when the shadow is no projected on the capture footprint [21].

The height is determined from the required spatial resolution or GSD; according to [30], 15 cm/px are required for quick inspections at panel string level, 5.5 cm/px for annual preventive inspections and 3.0 ± 0.5 cm/px for deep inspections, which, according to IEC TS 62446-3, can detect dirt and white spots at cell level [21].

It is recommended that thermal images are captured with georeferenced metadata (GPS coordinates) that facilitates their photogrammetric processing [21]. In the case of using ground control points for precise georeferencing, it is recommended to use aluminum markers, because in the thermogram they are observed in black color due to their low emissivity [21]. This represents an additional cost in material and time, however, in large facilities where the missions will be repeated and compared many times, this cost is justified [21].

According to [31], the camera's emissivity should be set to 0.90 for crystalline cells, and [15] recommends 0.85.

Concerning the flight speed, it should be low to avoid blurry images. In [32], good results were obtained at 1.0 m/s, in comparison to other experiments with higher speeds in the generation of RGB orthophotos. Of course, flight times must

be adjusted accordingly to the autonomy of the drone and area to be covered.

3. Case Study

A DJI Phantom 4 UAS with a FLIR Thermal camera was used to inspect a photovoltaic installation in operation, using the photogrammetric approach described in section 2. This section describes the site, the flight missions, and configuration settings used.

3.1. PV station analyzed.

The Tecnológico de Costa Rica (TEC) has in its campuses in Costa Rica PV installations with about 1,200 panels that are managed by the Laboratory of Electronic Systems for Sustainability (SESLAB); the energy generated is distributed to different facilities in the campuses [33]. For this article, the 19.4 kW PV station located in Santa Clara, San Carlos, was taken as the evaluation site (see Fig. 5), which has the following characteristics:

1) Configuration: 72 panels distributed in 6 strings of 12 panels in series (see Fig. 6), with 3 monocrystalline and 3 polycrystalline strings.

2) Dimensions: The panels are 1650 mm x 992 mm and the strings are 4.95 m x 3.97 m.

3) Geolocation WGS-84: 10.361085, -84.509056.

An RGB picture taken with the drone is shown in Fig. 6.

Fig. 5. Aerial photograph of TEC's photovoltaic station (identified in red) located in San Carlos. Source: Google Maps.

Fig. 6. Aerial photograph of the photovoltaic installation, where each string is identified.

3.2. Description of the UAV and thermal camera.

A commercial Phantom 4 Pro multirotor drone was the UAS platform, with a thermal camera attached. According to the manufacturer, the drone (see Fig. 7) weights 1388 g and a flight time of 30 minutes without the thermographic system.

Fig. 7. Drone with RGB and thermal camera used in this work.

To use the thermal camera with the drone, the following components were included: voltage regulator, 7" monitor (to view the camera image wirelessly), LIPO 3S battery, remote control for the thermal camera gimbal, and the FLIR VUE PRO R camera.

Table 1 shows the specifications of the thermal camera. The camera has a fixed focus set by the manufacturer. The color palette range is automatically adjusted to improve viewing; it cannot be adjusted manually.

Table 1. Characteristics of the FLIR VUE PRO R 336 thermal camera [34, 35].

Parameter	Value
HFOV x VFOV	25° x 19°
Sensor (width x height)	5.764 mm x 4.351 mm
Focal length	13.00 mm
Image width x height	336 x 256
Frequency	9 Hz
Weight	4 oz
Accuracy	+/- 5°C o 5% from reading
Spectral band	7.5 µm -13.5 µm
Size	57.4 mm x 44,45 mm x 44,45 mm
Input voltage	4.8 VDC - 6.0 VDC
Power dissipation (Peak)	2.1 W (3.9 W)
Thermal sensitivity	40 mK
Sensor	Uncooled microbolometer

3.3. Thermal camera setup

The camera was configured with the FLIR UAS 2 application. The configuration was done via Bluetooth, starting to take pictures before take-off and then turning off the Bluetooth to avoid interference with the mission. Table 2 shows the configured parameters.

Table 2. Parameters for image capture and thermographic analysis

Parameter	**Value**
Distance	24 m
Emissivity	0.9
Color palette	Fusion
Humidity	>60 %
Reflected temperature	22 °C
Average Atmospheric Temperature	30 °C
Interval between captures	1 s
File extension	RJPEG for Still Images / Tiff for Orthomosaic

3.4. Orientation used for the thermal camera.

To satisfy the premises indicated in section 2.4, the inclination of the panels α = 9° must be considered. The orientation used with respect to the vertical plane β + α was 30° (β = 21°) (see Fig. 8).

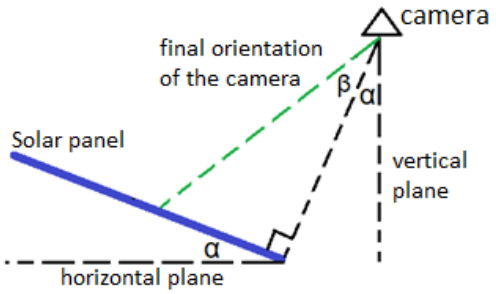

Fig. 8. Diagram of the orientation of the thermal camera relative to the solar panel.

3.5. Flight Plan.

The route of the mission was made manually following the recommendations in section 2.4. The route used is shown in Fig. **9**.

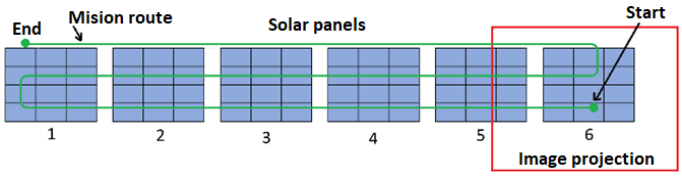

Fig. 9. Route employed in the infrared photogrammetry mission.

With Eq. (1) [36], the height to reach an effective GSD of 3.0 cm/pixel was determined.

$$h = (f_r \cdot Image_{width} \cdot GSD)/(100 \cdot S_W) \quad (1)$$

where f_r is the focal length of the image sensor, $Image_{width}$ is the footprint of the image on the panel and S_w is the size of the sensor. This was adjusted considering 1.3 m (see Fig. 10) of the solar minimum panel height, resulting in a maximum flight height (h) of 24 m from the take-off ground level.

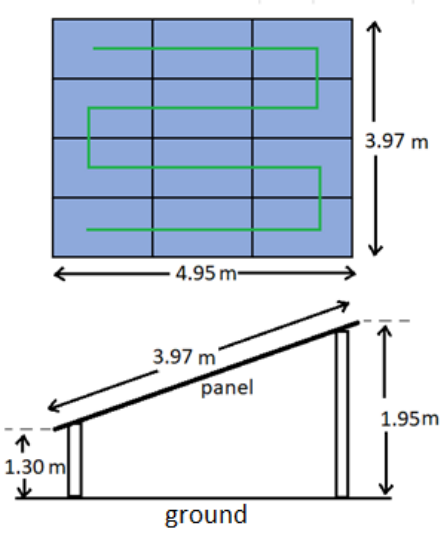

Fig. 10. Top and side view diagram of a solar panel string. The green line represents the way they are electrically interconnected

4. Results and discussion

4.1. Generation of the orthomosaic.

The mission reported here was performed on November 9, 2019, with the following considerations: flight height of 23.7 m, the thermal camera was turned on 60 min before the flight to achieve greater stabilization in the temperature of the camera, and the images began to be taken at 14:48 h local time with 96% battery and ended at 14:57 h with 32% of charge. Additional images were taken and the drone landed at 14:59 h with 20% of battery charge.

The weather was partially cloudy with an irradiance of 523 W/m2, the ambient temperature of the camera was set to 30 °C, and the drone flight speed was less than 1 m/s. Because the mission was manual with low flight speed, the effective overlap was greater than required (90%). Images were taken every second independently of the drone's operation, generating approximately 600 images during the mission. It was found that with a mission of 11 min the battery was consumed to 20% (remaining charge to switch to the "return to home" mode), showing that the autonomy decreases considerably from the 30 min indicated by the manufacturer under normal conditions (without the additional equipment for thermography measurement). For inspections in larger PV stations, multiple missions would be required or an alternative UAS platform with more flexible payload configuration or capacity could be used.

The data processing was done with Agisoft Metashape v1.5.5. Not required photos were manually removed, processing 525 images. A raster transformation was made (see Fig. 11 for the selected palette) and the processes shown in Table 3 were applied. The photogrammetric process allowed the generation of the orthomosaic in Fig. 12.

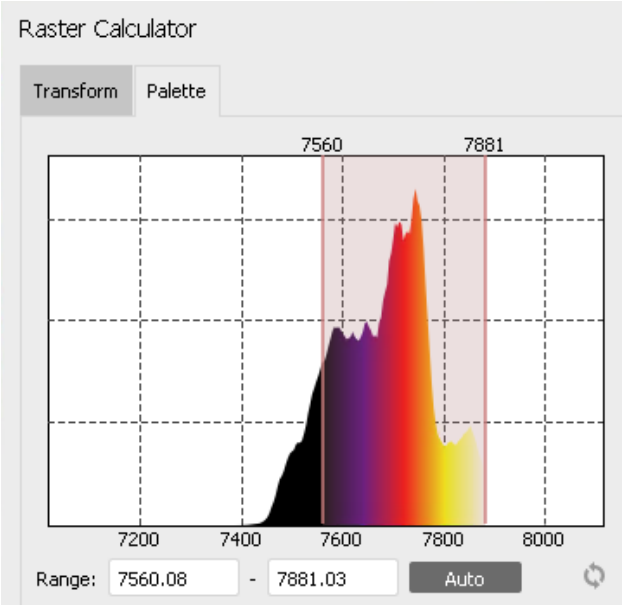

Fig. 11. Color palette assigned for raster processing. Source: image adapted from Agisoft Metashape.

Table 3. Parameters used for the creation of the orthomosaic.

Procedure	Parameters
Align photos	Accuracy: Highest Generic preselection Apply mask to: key points
Build dense cloud	Quality: High Depth filtering: Aggressive Calculate point colors
Build Mesh	Source data: Dense cloud Surface type: Height field (2.5D) Face count: High
Build Texture	Mapping mode: Orthophoto Blending mode: Mosaic Enable hole filling Enable ghosting filter
Build Tiled Model	Source data: Dense Cloud Face count: High Enable ghosting filter
Build Orthomosaic	Type: Planar Projection plane: Top XY Surface: Mesh Blending mode: Mosaic Enable hole filling

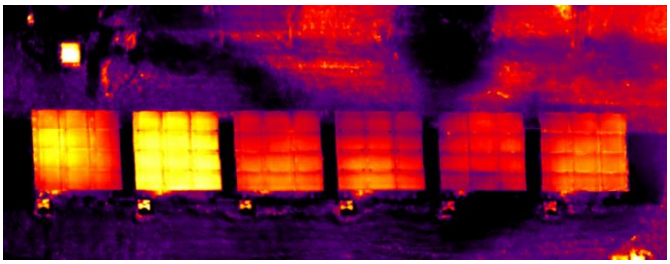

Fig. 12. Orthomosaic generated from the UAS mission.

This process was laborious, requiring masks to be placed on panel strings 1 and 5 due to variations in the tonality of the images by the self-calibration of the camera. A large number of images was used concerning the area covered, however, the processing time for the orthomosaic was 19 minutes with 11 seconds using a server with an Intel Xeon CPU X5675@3.07 GHz, 64 GB of RAM and 4 CUDA GPUs @ 849 MHz with 4096 MB of RAM; the process is relatively fast due to the low resolution of the thermal images in comparison to RGB images that usually require several MB per image.

The orthomosaic generated allowed the apparent temperature of the PV installation to be evaluated from a

qualitative point of view. String 2 was found to have a higher temperature than the others. On strings 5 and 6 a cell was identified as being hotter than its neighboring cells (see Fig. 13). With this, it is shown that the GSD of 3 cm/pixel used is sufficient to visualize thermal information at the cell level, which meets the requirements, mentioned in 2.4, to detect hot spots and partial shadows; however, this will be possible only if the orthomosaic has no distortion at the cell level. Regarding the heating of string 2, it was later found that the associated panels were not in operation due to an undetected failure in the main switch; this proved the possibility of detecting failures at string level.

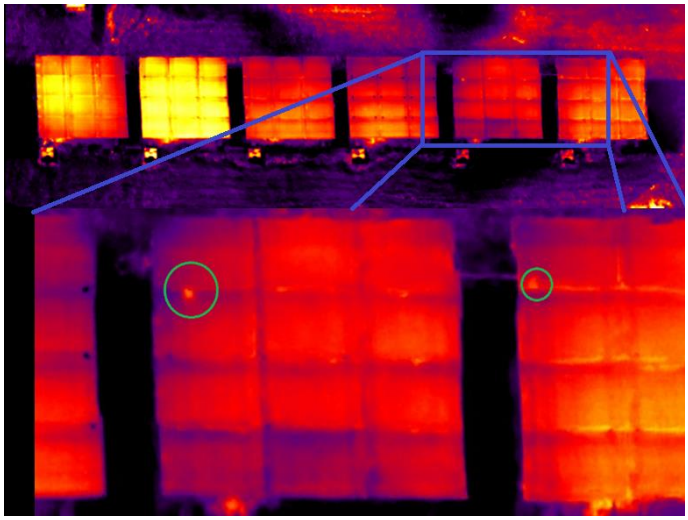

Fig. 13. Identification of cells with higher temperature (indicated in green) in the orthomosaic for string 5 (left) and string 6 (right).

The image processing presented difficulties due to the variation in the tonality of consecutive images due to automatic self-calibration of the camera. Therefore, it is important that the environmental conditions during the mission do not change considerably to avoid obtain different color maps within the images. Although the images could be pre-processed to balance the maps, this issue requires further analysis in future work.

4.2. Individual images.

Since the color map after the photogrammetric process might vary from the actual scale associated with certain temperature levels, after the general inspection it was required to acquire single images at the points where anomalies were detected.

A second mission to collect these additional images was performed on October 29, 2019, using the same protocol as for the orthomosaic mission; about 57 images were taken during the flight, the weather was clear with irradiance between 535 W/m2 - 633 W/m2, the ambient temperature in the camera was set to 30 °C. The image processing was done with the *Flir Tools* application. Forty images were selected, which allowed an analysis of the condition of each string. Two of the processed images are shown in Fig. 14 and Fig. 15.

The results of the individual images are in conformity with those of the orthomosaic since it was also qualitatively identified that strings 5 and 6 have a warmer cell (Fig. 14); the quantitative analysis shows that the cells with higher temperature have a variation of less than 3 °C from those with normal temperature, which is within the expected normal operation range. It was also possible to identify the higher heating of the entire string 2 with respect to the 3 (Fig. 15).

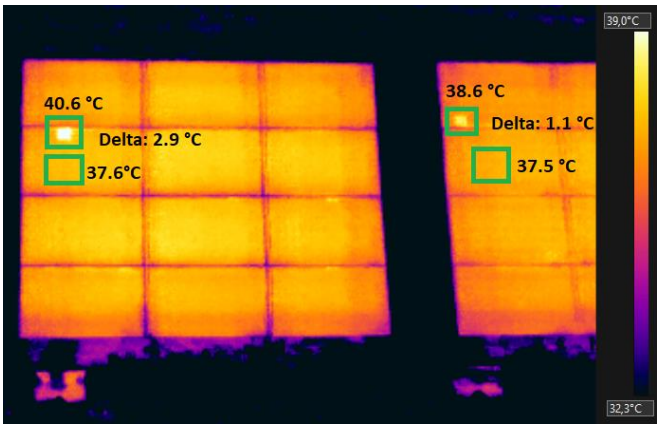

Fig. 14. Thermal image of strings 5 and 6 (from left to right). Two cells are displayed with a higher temperature which after a quantitative analysis indicates a temperature differential of 2.9 °C (left) and 1.1 °C (right).

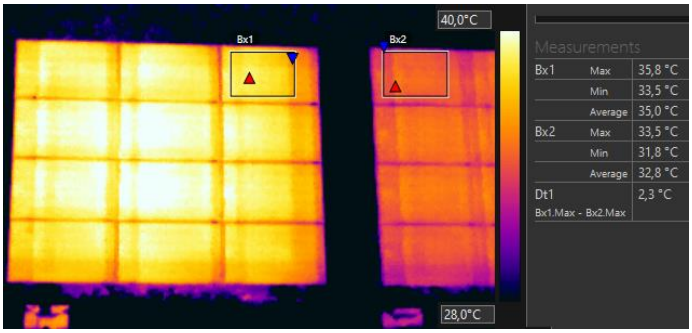

Fig. 15. Thermal image analysis of strings 2 and 3 (from left to right) using Flir Tools software

4.3. Result validation

To validate the thermography estimations, it is possible to perform direct temperature measurements with thermocouples [37, 38], keeping in mind that the aim is not to find the same temperature measurements, since this would require that the measurements be simultaneous to ensure the same environmental conditions, however, the temperature variations must be consistent. To address this, the following procedure was applied between Feb. 27 and March 5, 2020:

a) In strings 5 and 6, measurements were taken with a thermocouple on the back of the hot cell (the cell with the highest temperature in the thermogram) and of another cell with normal temperature. The results are shown in Table 4.

b) An additional thermogram was taken on string 2 (Fig. 16) after correcting the fault detected in the main switch. In this new experiment, a new hot point was found, for which a thermocouple temperature measurement was made to validate the new thermogram (see Table 5).

Table 4. Temperature of the hottest cells identified in strings 5 and 6. On-site irradiance was between 773 W/m^2 and 830 W/m^2.

String	Temperature measured with thermocouple [C°]		
	Hot cell	Reference cell	Difference
5	45	38	7
6	44	41	3

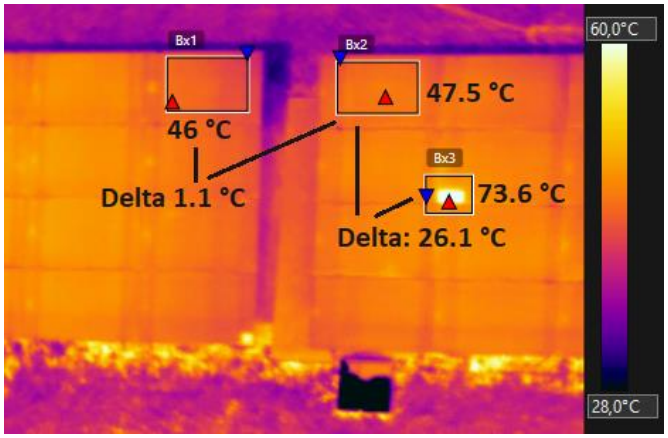

Fig. 16. Analysis of the thermograph of string 1 (left) and string 2 (right) after repairing the false contact in the main switch of string 2.

Table 5. Hot spot measurements of string 2 by thermography and contact measurement.

Measuring mechanism	Temperature (°C)			
	Hot cell	Cold Cell	Difference	Irradiance (W/m^2)
Thermography	73.6	47.5	26.1	932
Contact measurement	65	39	26	886

Table 4 shows that the thermocouple measurement in the hot cells of strings 5 and 6 have a temperature difference of up to 7 °C, in contrast to the thermography where the difference was less than 3 °C (Fig. 14). This is to be expected because the irradiance was higher during thermocouple measurements, which generates more heating in the panels [24]. The results are satisfactory, as they agree with the diagnosis that there is no failure until a difference of 10 °C is present, as mentioned in Section 2.1.

The thermogram of string 2 after correcting the fault in the main switch (Fig. 16) shows a difference of 1.1 °C with respect to a neighbouring string, whereas, with the fault present, it was 2.3 °C (Fig. 15). This indicates that a small temperature increase between strings may indicate a fault, in this case, an open circuit.

The cell with the highest temperature identified in string 2 shows, both with the thermograph and with the thermocouple measurement, a difference in temperature higher than 26 °C (see Table 5), which tells that the quantitative information of the thermograph allows to effectively detect a failure at the cell level.

4.4. Comparison between orthomosaic and individual images

It can be stated from the previous evaluation that the uncalibrated orthomosaic can provide a general overview of the installation, and allows to identify suspicious areas where fails might occur. However, this approach in its current form does not provide precise quantitative information.

In contrast, with individual thermograms, it is possible to obtain quantitative data but without being able to observe the full installation, and this approach can be used as a second pass to inspect suspicious areas observed in the orthomosaic. This means that both, the photogrammetric analysis and thermogram are required and can be viewed as complementary tools to achieve a precise evaluation of a photovoltaic installation.

Although the minimum irradiance conditions indicated in section 2.4 were assured, the greater the irradiance present at the site, the greater the thermal contrast will be when a failure exists [24]; however, this can be a challenge at sites with varying climatic conditions, such as this research site.

5. Conclusions

The results showed that with relatively low-cost equipment it is possible to achieve the necessary autonomy and precision requirements to detect failures, due to hot spots for instance, or inadequate operating conditions such as partial shadows in crystalline silicon photovoltaic installations. The presented approach is very useful in the management of photovoltaic installations, as it may allow extending the life of the system, which also can improve the return of investment and contribute to sustainable development.

Using the applied methodology, individual images allowed detecting failures with reliable quantitative information, although with the difficulty of identifying the string of interest and not achieving a vision of the complete installation. In contrast, the orthomosaic showed a complete picture of the PV installation with a good resolution, enabling qualitative analysis that guided the detection of possible failures at the cell level, identifying the string of interest easily.

Good correlation of thermograms with respect to thermocouples measurements on the panels could be observed. This is a useful resource as a complement to the general uncalibrated orthomosaic obtained through photogrammetry.

The qualitative information of the orthomosaic is useful but can also lead to false positives, as in the case here that two spots on the orthomosaics of strings 5 and 6 were discarded after evaluation of the thermogram. The self-calibration of the thermal camera made it difficult to generate orthomosaic with even color scales, even after giving one hour for stabilization of the temperature in the camera.

The autonomy and stability of the small scale drone used are significantly affected by the inclusion of additional equipment for thermography; therefore, for larger installations, a larger GSD would be necessary or many consecutive missions would be required to cover the entire area. Other UAS platforms with more flexible management of the payload in the same range of price could solve this issue for larger installations.

Future work will address photogrammetric surveying with autonomous flight missions, to reduce the number of images and consequently the mission execution and data processing times. Calibration of the processed orthomosaics, to adjust color maps to actual temperature values, is also a topic for further investigation.

Acknowledgements

This paper is part of a project 5402-1360-4201 “Identificación de Fallas en Sistemas Fotovoltaicos” financed by the Costa Rica Institute of Technology.

References

[1] J. J. Watson and M. D. Hudson, "Regional Scale wind farm and solar farm suitability assessment using GIS-assisted multi-criteria evaluation," *ScienceDirect*, vol. 138, pp. 20-31, 2015.

[2] S. Gallardo-Saavedra, L. Hernández-Callejo and O. Duque-Perez, "Image Resolution Influence in Aerial Thermographic Inspections of Photovoltaic Plants," *IEEE Transactions on Industrial Informatics*, vol. 14, no. 12, pp. 5678-5686, 2018.

[3] W. Chine, A. Mellit, V. Lughi, A. Malek, G. Sulligoi and A. Massi Pavan, "A novel fault diagnosis technique for photovoltaic systems based on artificial neural networks," *Renewable Energy*, vol. 90, pp. 501-512, 2016.

[4] L. D. Murillo-Soto and C. Meza, "Diagnose Algorithm and Fault Characterization for Photovoltaic Arrays: A Simulation Study," in *Springer Lecture Notes in Electrical Engineering (ELECTRIMACS 2019)*, vol. 604, Zamboni W., Petrone G, Springer, Cham, 2020, pp. 567-582.

[5] A. Mellit, G. Tina and S. Kalogirou, "Fault detection and diagnosis methods for photovoltaic systems: A review," *Renewable and Sustainable Energy Reviews*, vol. 91, pp. 1-17, 2018.

[6] T. J. Silverman, L. Mansfield, I. Repins and S. Kurtz, "Damage in Monolithic Thin-Film Photovoltaic Modules Due to Partial Shade," *IEEE Journal of photovoltaics*, vol. 6, no. 5, pp. 1333-1338, 2016.

[7] H. Mekki, A. Mellit and H. Salhi, "Artificial neural network-based modelling and fault detection of partial shaded photovoltaic modules," *Simulation Modelling Practice and Theory*, vol. 67, pp. 1-13, 2016.

[8] S. Choudhury and P. Rout, "AdaptiveFuzzy Logic Based MPPT Controlfor PV System underPartial Shading Condition," *International Journal of Renewable Energy Research*, vol. 5, no. 4, pp. 1252-1263, 2015.

[9] M. Davarifar, A. Rabhi, A. Hajjaji, E. Kamal and Z. Daneshifar, "Partial shading fault diagnosis in PV system with discrete wavelet transform (DWT)," in *2014 International Conference on Renewable Energy Research and Application (ICRERA)*, Milwaukee, WI, USA, 2014.

[10] M.-R. Fazal, Z. Abbas, M. Kamran, I.-u. Haq, M.-N. Ayyaz y M. Mudassar, «Modified Perturb and ObserveMPPT Algorithm for Partial Shading Conditions,» *International Journal of Renewable Energy Research*, vol. 9, nº 2, pp. 721-731, 2019.

[11] J. A. Tsanakas, L. Ha and C. B. , "Faults and infrared thermographic diagnosis in operating c-Si photovoltaic modules: A review of research and future challenges," *Renewable and Sustainable Energy Reviews*, vol. 62, pp. 695-709, 9 2016.

[12] Y. Zhao, "Fault detection, classification and protection in solar photovoltaic arrays," Ph.D. Dissertation, Dept. of Electrical and Computer Engineering, Northeastern University, 2015.

[13] S. Saee, F. Gohar Awa, M. Nasir, M. Mudassa, M. Kamran, A. Nazir and W. Naza, "Analysis of Interconnection Schemes for PV Systems Operating under Shadow Conditions," *International Journal of Renewable Energy Research*, vol. 9, no. 2, pp. 913-922, 2019.

[14] A. Gutierrez, M. Bressan, J. Jimenez and C. Alonso, "Development of real-time supervision HIL emulator of shaded PV systems," in *2017 IEEE 6th International Conference on Renewable Energy Research and Applications (ICRERA)*, San Diego, CA, USA, 2017.

[15] IEA International Energy Agency, «Review of Failures of Photovoltaic Modules,» Performance and Reliability of Photovoltaic Systems, 2014.

[16] S. S. Siva Ramakrishna Madeti, "A comprehensive study on different types of faults and detection techniques," *Solar Energy*, pp. 161-185, 2017.

[17] M. Alsafasfeh, I. Abdel-Qader and B. Bazuin, "Fault Detection in Photovoltaic System Using SLIC and Thermal Images," in *2017 8th International Conference on Information Technology (ICIT)*, IEEE, 2017.

[18] A. Y. Appiah, X. Zhang, B. B. K. Ayawli and F. Kyeremeh, "Review and Performance Evaluation of Photovoltaic Array Fault Detection and Diagnosis Techniques," *International Journal of Photoenergy*, no. 6953530, 2019.

[19] S. Vergura, F. Marino and M. Carpentieri, "Processing infrared image of PV modules for defects classification," in *2015 International Conference on Renewable Energy Research and Applications (ICRERA)*, Palermo, Italy, 2015.

[20] Y. Higuchi and T. Babasaki, "Failure detection of solar panels using thermographic images captured by drone," in *2018 7th International Conference on Renewable Energy Research and Applications (ICRERA)*, Paris, France, 2018.

[21] Y. Zefri, A. ElKettani, I. Sebari and S. Ait Lamallam, "Thermal Infrared and Visual Inspection of Photovoltaic Installations by UAV Photogrammetry—Application Case: Morocco," *drones*, vol. 2, no. 4, p. 41, 23 11 2018.

[22] W. Yadong, . t. Kazutaka, . u. Tsugutomo, K. Keishin and G. Qiang, "Voltage-Based Hot-Spot Detection Method for Photovoltaic String Using a Projector," *energies*, vol. 10, no. 2, p. 230, 2017.

[23] R. Moretón, E. Lorenzo and L. Narvarte, "Experimental observations on hot-spots and derived acceptance/rejection criteria," *Solar Energy*, vol. 118, pp. 28-40, 2015.

[24] M. Cubukcu and A. Akanalci, "Real-time inspection and determination methods of faults on photovoltaic power systems by thermal imaging in Turkey," *Renewable Energy*, vol. 147, pp. 1231-1238, 2020.

[25] T. Yamamoto, D. Wagi and I. Nanno, "New Coupled Model for Prediction of the Temperature Distribution in a PV Cell with a Hot Spot Induced by Partial Shading," in *2018 7th International Conference on Renewable Energy Research and Applications (ICRERA)*, Paris, France, 2018.

[26] A. S. Chaudhary and D. K. Chaturvedi, "Analyzing defects of solar panels under natural atmospheric conditions with thermal image processing," *International Journal of Image, Graphics and Signal Processing*, vol. 10, no. 6, p. 10, 2018.

[27] A. Dolara, G. C. Lazaroiu and E. Ogliari, "Efficiency analysis of PV power plants shaded by MV overhead lines," *International Journal of Energy and Environmental Engineering*, vol. 7, no. 2, pp. 115-123, 2016.

[28] S. Arriola-Valverde, K. Villagra-Mendoza, M. Méndez-Morales, M. Solórzano-Quintana, N. Gómez-Calderón and R. Rimolo-Donadio, "Desarrollo y Validación de una Metodología para la Cuantificación de la Erosión Hídrica a través de Fotogrametría UAS," *Revista Tecnología En Marcha*, vol. 32, no. 5, pp. 43-52, March 2019.

[29] S. Arriola-Valverde, K. Villagra-Mendoza, M. Méndez-Morales, M. Solórzano-Quintana, N. Gómez-Calderón and R. Rimolo-Donadio, "Analysis of Crop Dynamics Through Close-Range UAS Photogrammetry," in *Food CAS, IEEE International Symposium on Circuits and Systems*, Seville, Spain, 2020.

[30] FLIR, "A guide to inspecting solar fields with thermal imaging drones," 16 07 2019. [Online]. Available: https://thermalcapture.com/wp-content/uploads/2019/08/pv-system-inspection-thermal-drones-07-15-19.pdf. [Accessed 11 06 2020].

[31] A. Riverola, A. Mellor, D. A. Alvarez, L. F. Llin, I. Guarracino, C. N. Markides and N. Ekins-Daukes, "Mid-infrared emissivity of crystalline silicon solar cells," *Solar Energy Materials and Solar Cells*, vol. 174, pp. 607-1615, 2018.

[32] G. Y. Jeong, T. N. Nguyen y D. K. Tran, «Applying unmanned aerial vehicle photogrammetry for measuring dimension of structural elements in traditional timber building,» *Measurement*, vol. 153, p. 107386, 2020.

[33] C. Meza, H. Sanchez, F. Monge, J. Morera and A. Mendez, "Estrategia para la implementación de iniciativas sostenibles en ciudades universitarias ejemplificada con el Complejo Solar del TEC de Costa Rica," in *II Ibero-Ameriacan Congress of Smart Cities (ICSC-CITIES2019)*, Soria, Spain, 2019.

[34] Flir, "Flir Vue Pro and Flir Vue Pro R," 2019. [Online]. Available: http://www.flir-vue-pro.com/wp-content/uploads/2016/10/FLIR-VUE-Pro-R-Datasheet-TeAx.pdf. [Accessed 11 06 2020].

[35] Flir.com, "Adjusting Sensitivity & Gain On The FLIR Vue Pro R," Flir, 10 10 2019. [Online]. Available: https://flir.custhelp.com/app/answers/detail/a_id/3134. [Accessed 09 07 2020].

[36] W. Linder, "Introduction," in *Digital Photogrammetry*, 4 ed., Springer-Verlag Berlin Heidelberg, 2016, pp. 10-12.

[37] D. Anthony, D. Sarkar and A. Jain, "Contactless, non-intrusive core temperature measurement of a solid body in steady-state," *International Journal of Heat and Mass Transfer*, vol. 101, pp. 779-788, 2016.

[38] E. Rodriguez, J. Mireles, C. A. Terrazas, D. Espalin, M. A. Perez and R. B. Wicker, "Approximation of absolute surface temperature measurements of powder bed fusion additive manufacturing technology using in situ infrared thermography," *Additive Manufacturing*, vol. 5, pp. 31-39, 2015.

Article 2.

Experimental comparison of visual inspection and infrared thermography for the detection of soling and partial shading in photovoltaic arrays.

Publisher: Springer International Publishing

Book title: Smart Cities

Book Subtitle: Third Ibero-American Congress, ICSC-Cities 2020, San José, Costa Rica, November 9-11, 2020, Revised Selected Papers

Authors: Cardinale-Villalobos, L., Meza, C., & Murillo-Soto, L. D

Year: 2020

Series Volume: 1359

Indexed in Scopus

Experimental comparison of visual inspection and infrared thermography for the detection of soling and partial shading in photovoltaic arrays

Leonardo Cardinale-Villalobos[1 [0000−0002−9649−6017]], Carlos Meza[1 [0000−0002−7374−505X]], and Luis Murillo-Soto[2 [0000−0002−6601−1082]]

[1] Electronics Engineering School, Instituto Tecnológico de Costa Rica, Costa Rica
lcardinale@tec.ac.cr
[2] Electromechanic Engineering School, Instituto Tecnológico de Costa Rica, Costa Rica

Abstract. Soling and partial shading of solar panels are two of the most common conditions that affects the power yield of a photovoltaic (PV) installation. Even though human inspection can easily identify such situations, in the case of large power plants covering thousands of hectares it is not practical. In this regard, unmanned areal systems (UAS) represents a useful tool to gather images in a short time for the inspection of thousands of PV panels. Using RGB and infrared cameras, UAS can be used to perform visual inspection (VI) and infrared thermography (IRT) to detect failures in PV arrays. The present paper presents the results of an experiment designed to evaluate the effectiveness of VI and IRT for detecting soiling and partial shadowing. It has been found that for the aforementioned conditions VI are more effective. Also, the methodology presented can be used as a reference for future research for other techniques and other failures. The results provide technical-scientific information for those in charge of operation and maintenance to make an objective choice of failure detection techniques.

Keywords: Solar PV System · Fault detection performance · Partial shading · Soiling · Thermography

1 Introduction

A photovoltaic (PV) power plant is capable of operating for more than 25 years and due to its low energy density the installations can occupy thousands of hectares [38]. A group of PV panels are connected in series to form strings and, in some cases, in parallel to form arrays injecting the generated energy through a power inverter. Weather, soling and obstacles that produces shadows yield suboptimal conditions in the PV array, i.e., the group of PV panels produces less power than expected. In the case of soling or obstructing elements the suboptimal condition can be corrected if detected. In this regard, strategies related to the operation and maintenance of PV modules acquired greater importance. Even though such conditions can be identified by human operators, as reported in [12],

expert visual inspection and fault analysis in a 3 MW installation take 60 days. Thus, developing techniques that detects such suboptimal conditions in shorter time becomes a necessity.

There are several techniques to identify faults and suboptimal techniques, e.g. [37], [9], [5], [32], [22], [17], [20], [12], [4], [30], [29]. Two of the most promising are based on imaging, given that these techniques do not require to intervene the PV power plant circuit, does not require contact with the element of interest and generates a large amount of qualitative and quantitative information for each image. Such images can be taken in a relative short time if unmanned aerial systems (UAS) are used. UAS also known as drones with onboard thermal cameras enable inspections from the air and through digital photogrammetry techniques it is possible to detect failures in an agile way (e.g., [15], [36]).

The camera attached to the UAS can be of the type that captures the red, green, blue (RGB) band or the infrared band. With an infrared band detection camera it is possible to obtain thermal images of solar panels which allows the identification of temperature gradients or hot spots that can be associated with panel failures [2,23]. Such technique is referred as infrared thermography (IRT).

The present paper compares two drone image-based fault detection techniques: (1) visual inspection (VI) based on RGB images and (2) a strategy based on IRT through infrared images. An experiment has been designed to measure the performance of the aforementioned techniques for partial shadowing and soiling, which represents two of the most common suboptimal techniques. The rest of the paper is structured as follows: firts the suboptimal conditions considered are described, then the material and methods are presented. Section 4 presents the main results and section 5 gathers the main conclusions.

2 Suboptimal conditions considered

For the comparative analysis we consider the following suboptimal conditions:

- Partial shadowing: The power generated by a series of solar panels will suffer a decrease in the power generated when they are partially shaded [27]. Partial shading can be caused by objects located in the surface on the panel or by objects not in contact with the panel. The power affectation depends on the portion of the module that is shaded and on the degree to which it is shaded [24,31]. An example of a shadowed panel is shown in Fig. 1.

- Soiling: can be caused due to the presence of a thin layer of particles such as soil, dust, leaves, pollen or bird droppings [24]. The PV power affectation is greater as the soiling increases. A dirty PV module is shown in Fig. 2. Soling can be uniform or non-uniform. Dirt due to dust consists of particles of different sizes and materials that cover the entire PV module, which, over time, will form uniform layers of dust and regions with greater accumulation of dirt [18]. Non-uniform dirt covering only some cells of the PV module, due to leaves, bird droppings or patches of soil have a severe power loss effect, this type of failure is associated with both soiling and partial shading. PV

cells that capture less irradiance have a lower short circuit current than the rest, causing the entire module to deliver less current. In addition, dirty cells will cause a hot spot that can be detected with IRT [24].

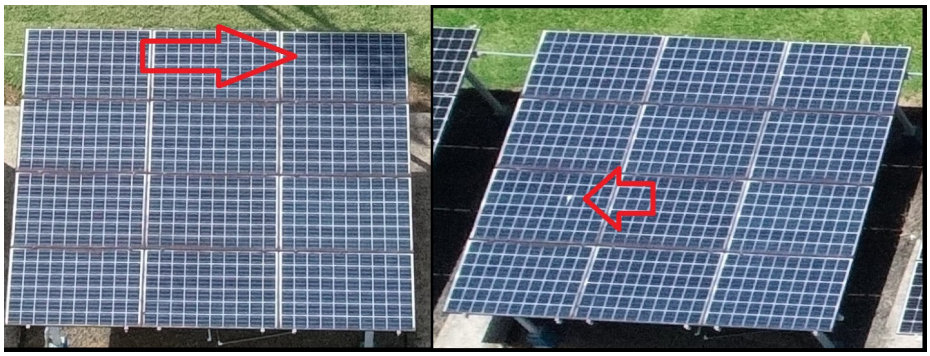

Fig. 1. Partial shadow on a PV panel (left) and strange object on a PV panel (right).

Fig. 2. Soiled PV module.

3 Materials and methods

3.1 The PV installation analyzed

The data used to compare VI and IRT suboptimal detection techniques consisted of images from a ground mounted PV installation located in Santa Clara, Costa Rica. The details of the PV installation are shown in Table 1.

Table 1. Information about the PV installation analyzed

Longitude	-84.51
Latitude	10.36
Azimut angle	0° with respect to the South
Inclination angle	15°
Peak DC power	19.4
Number of PV panels	72
PV panel models	Canadian Solar CS6k-280M and HANWHA Q-Cells QPRO BFR G4.3
Total surface (m^2)	125
Performance factor (%)	77.7
Annual Yield (MWh)	28.69
Date of commissioning	May 31st, 2017

Figure 3 shows an aerial view of the PV installation considered, where it can be seen that the site consists of six well distinguished sections. Each section has a string of 12 PV modules connected to an inverter SMA Sunny Boy 3000TL-US. In this analysis only strings 2, 4, and 6, shown in Fig. 3, were used. The aforementioned strings have a direct current STC power of 3380 W.

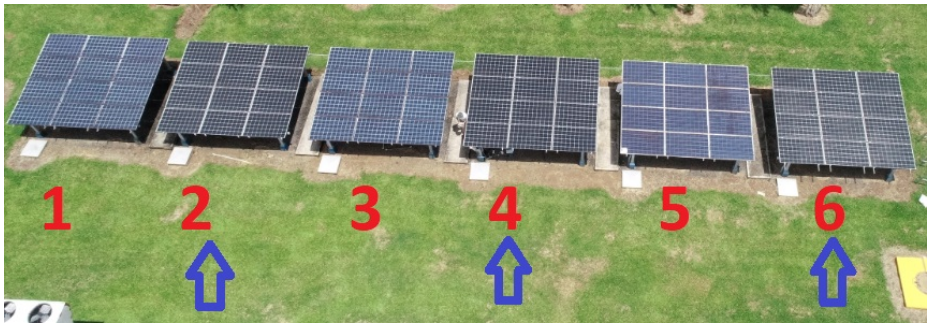

Fig. 3. Picture of the PV installation. Strings 2, 4 and 6 were used in this research.

3.2 Image capturing

The data used to determine the suboptimal conditions in the PV installation consisted of images taken from an (UAS). The following considerations have been considered to take the images:

– The drone is always flown at a height greater than 5 m to avoid that it causes shadows on the panels [20].

– The flight height depends on the detail that is necessary to observe in the PV modules for proper fault detection, thus, the size of the fault has been taken into account to determine the spatial resolution require for the images taken in a drone mission (ground sampling distance (GSD) [8]). A GSD of 3.0 ± 0.5 cm/px is required for deep inspections [9], allowing to detect possible hot spots at cell level [4].
– The measurements were made at a time with sufficient irradiance to allow the capture of thermal contrasts, with a correct angle and without wind currents that generate convection cooling [40], constant sunlight conditions with a clear sky are also desirable so that solar panels in good conditions have a homogeneous thermal distribution [36].
– The images were captured with an angle between 5°and 60°with respect to the perpendicular of the panel (see Fig. 4) [40] and the irradiance was always greater than $700 \mathrm{W/m^2}$ [16]. The camera's emissivity was set to 0.85 for crystalline cells as indicated in [17].
– The drone was set to consecutive image capture as recommended in [37, 40] for fault detection in PV installations.

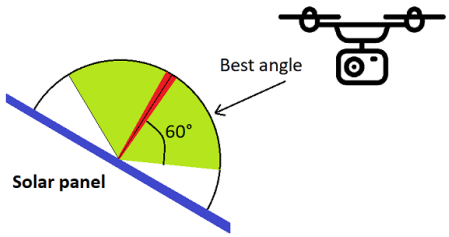

Fig. 4. Recommended orientation of the thermal camera with respect to the panel position.

A commercial Phantom 4 Pro multirotor drone was used as the UAS platform (see Fig. 5). The characteristics of the RGB and thermal infrared camera are shown in Table 2 and 3, respectively.

Table 2. Characteristics of the RGB camera used

Parameter	**Value**
Sensor	1" CMOS/ Effective pixels 20M
Lens	FOV 84° 8.8 mm/24mm
PIV Image Size	4096 x 2160
Photo	JPEG
Image Size	3:2, 4:3, 16:9
ISO Range	100-3200 (Auto)

Fig. 5. Drone with RGB and thermal camera used in this research.

Table 3. Characteristics of the FLIR VUE PRO R 336 thermal camera [10, 11]

Parameter	**Value**
HFOV x VFOV	25°x 19°
Sensor (width x height)	5.764 mm x 4.351 mm
Focal length	13.00 mm
Image width x height	336 x 256
Frequency	9 Hz
Accuracy	+/- 5 °C o 5% from reading
Thermal sensitivity	40 mK
Sensor	Uncooled microbolometer

3.3 Other instruments and measurements

On-site irradiance was measured with a Spektron 210 sensor and the ambient temperature and relative humidity from a Vantage Pro 2 weather station. The power from the inverters was taken from the built-in SMA data logging system. A schematic of the system is shown in Fig. 6.

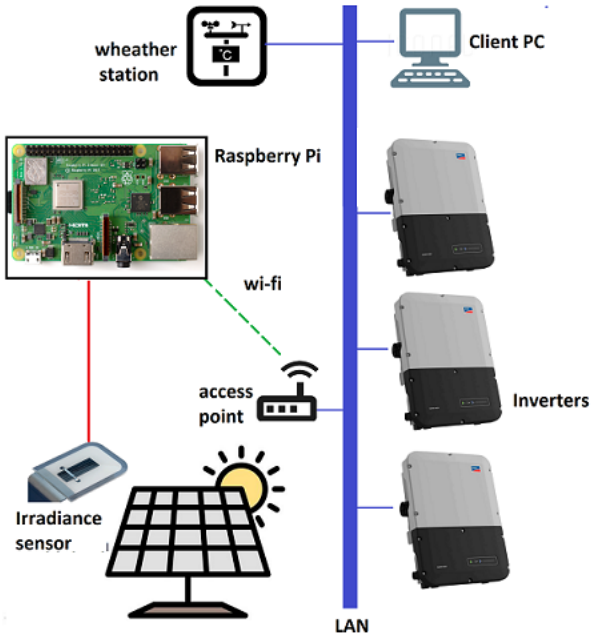

Fig. 6. Schematic diagram of communication links to information sources.

3.4 Experiments

The research was developed through a case study applying an experiment. Predefined temporary suboptimal conditions were induced to the PV installation in operation which allowed collecting and processing quantitative information to compare the IRT and VI techniques through statistical analysis. Taking as reference [14, 39] the following stages were used:

- Selection of the sample and information sources.
- Design of the experiment.
- Definition of protocols and criteria for the interpretation of results.

The experiment used a repeated measurement design because multiple treatments had to be applied to the same subjects [35]. A total of 28 experimental

units were analyzed from the 8 treatments applied to the 2 subjects (Strings 4 and 6). String 2 was used as a control subject to establish a reference condition in each experimental unit for the normal operation of the PV strings, i.e. without applying failures. The factors and levels evaluated are shown in Table 4.

Table 4. Factors and levels used in the experiment to generate the diverse treatments.

Failure	Factor	Level
S1	Soiling	10 months of natural soil
S2		30 months of natural soil
S3		12 cells with white spots
S4		12 cells with dry leaves from the site
S5		21 cells with white spots
S6		21 cells with dry leaves from the site
PS1	Partial shading	Shading of approximately 70% of a panel's area
PS2		2 shadows, each approximately 30% of the area of a panel

The treatments were applied to the subjects without interaction between factors. Each level was applied in both subjects making two repetitions in each one. The selection of the modules of each string to which the failure was applied was chosen at random. The partial shadows were limited to the modules on the right margin due to site conditions. It was considered that there is an independent relationship between the treatments, because they were randomized and do not generate a residual effect in the subject [13], i.e., the PV string return to their normal state once the treatment is removed.

3.5 Description of each factor and the levels of the experiment

– **A. Soiling**

Table 4 describes the dirt conditions used for faults S1 - S6. Faults S1 and S2 allowed the generation of soil conditions that cause weak shading [24]. Natural dirt accumulated in the solar panels over time was used as suggested in [18] which states that it is possible to take as an indicator of soiling the exposure time that the module has been under natural conditions.

Failures S3 and S5 were made to generate a strong obstruction of the irradiance due to some strange object on the solar panel. Samples of glass of 480 mm x 160 mm x 5 mm were prepared in which white paint was placed to simulate dirt on the PV module (see Fig. 7); this allowed to replicate the treatments in multiple moments in different positions of the PV array. The experiment took as a reference the methodology used in [34] to study the effects of dirt on solar modules.

Faults S4 and S6 are a variation of S3 and S5 to evaluate soiling. In this case, dry leaves and seeds were used, where to achieve repeatability in the experiment the objects were adhered to the glass with cold silicon (see Fig. 8).

Fig. 7. Glass with white circles used to simulate dirt obstructing the path of radiation in three PV cells.

Fig. 8. Glass with dry leaves and seeds to simulate dirt obstructing the radiation path in three PV cells.

– **B. Partial shading**

The experiment was developed by applying shadows to the solar modules in operation. The methodology took as reference experiences of previous investigations, in which, they placed an object to obstruct the solar radiation of a portion of the solar module, allowing that it influences diffuse radiation [26]. The two partial shading levels (PS1 and PS2) applied were made by placing an object next to the PV string to create the shadow (Fig. 9).

3.6 Protocol for missions with UAS

As mentioned previously, for each treatment a flight was performed with the UAS capturing RGB and infrared images of the PV strings of interest ensuring that the requirements indicated in section 3.2 were met. The flight height was 25 m according to the GSD equation presented by [21] to obtain a maximum GSD of 3.0 cm/pixel in thermal images and even less in RGB images.

The thermal images were configured to contain the radiometric information in RJPEG format. Thermographs were taken every 1 s and RGB images every 2 s during each test. The orientation of the cameras with respect to the perpendicular plane of the module was around 20 °C.

For each test, the irradiance, ambient temperature and relative humidity were recorded. Each treatment was applied 15 minutes before the measurement was taken to ensure that thermal equilibrium existed [17].

Fig. 9. Example of partial shadows generated on the PV modules.

3.7 Fault detection criteria

The temperature variation due to a hot spot is an indicator of the severity of the fault, where less than 10 °C is considered within the normal operation tolerance [16, 28] however, at lower irradiance, the temperature variation of a fault will decrease [7].

Fault detection in PV installations by VI can be done following the detailed guidance of [32]. For example, it is possible to identify soiling by evaluating the appearance of the solar modules so that it is classified as: clean, slightly dirty or very dirty. Furthermore, the dirt can be classified according to its location as: close to the frames or located somewhere on the glass (e.g. bird droppings). Partial shadows can be identified by observing the glass surface of the PV module.

According to the literature review, the criteria for the detection of the failures of interest for the applied techniques were determined. The criteria used are shown in the Table 5.

Table 5. Criteria used for the determination of failures

Technique	Criteria for fault detection
IRT	Hot spot with a delta $\geq$ 10 °C
VI	Presence of radiation attenuation on the panel due to shade
	Appearance of light or heavy soiling

3.8 Date and conditions of the experiment

All measurements were made between august 18 and september 2, 2020. The average ambient temperature was 30 °C, the relative humidity 60 % and the reflected temperature 22 °C.

3.9 Measurement normalizing

The three mono-crystalline strings are equivalent, however, their output power may vary slightly, so the power of the strings under test (String 4 and String 6) were compared with the control String 2 to set a reference level. Table 6 shows the variation in the average output power under non-fault conditions after two hours of operation with an irradiance greater than $700\,\mathrm{W/m^2}$.

Table 6. Power comparison of the string under test with respect to the control string

String	Power (W)	Variation (%)
2 (control)	2549	-
4	2566	0.67
6	2534	-0.59

4 Results and discussion

The results of the induced suboptimal conditions are shown in Table 7. Each one of the induced condition was considered as a fault because it caused a decrease of at least 4 % in the power of the array [1].

Table 7. Power effect of the faults studied

Fault (String)	Power in control string (W)	Power in string under test (W)	Estimated power without fault (W)	Losses (%)
PS1 (4)	2224	1920	2239	14.2
PS2 (6)	3133	2746	3115	11.9
S1 (4)	2137	1879	2151	12.7
S2 (6)	2137	1461	2124	31.3
S3 (6)	2421	1994	2407	17.1
S4 (4)	2421	1749	2437	28.3
S5 (6)	2094	1648	2082	20.8
S6 (4)	2094	1573	2108	25.4

4.1 RGB and IR images analysis

The most representative images that identifies suboptimal conditions are shown in Fig. 10 to 15. For each experimental unit, a discrete output variable was generated to indicate whether or not the technique detected failure; the results are shown in Table 8.

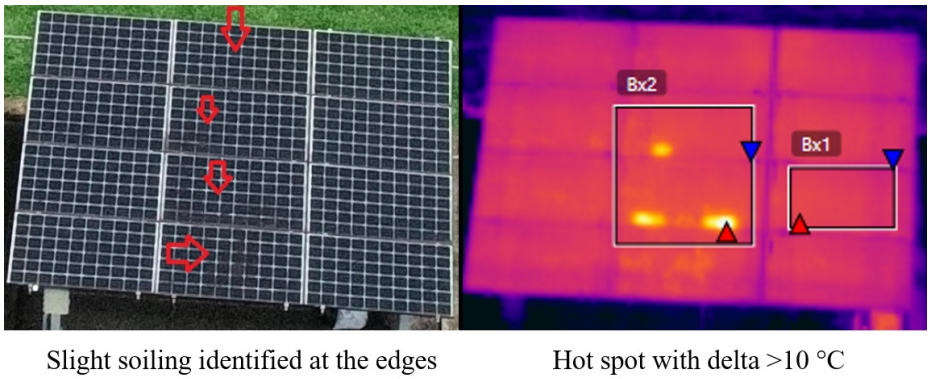

Fig. 10. RGB (left) and IR image (right) analyzed for experimental unit 1.

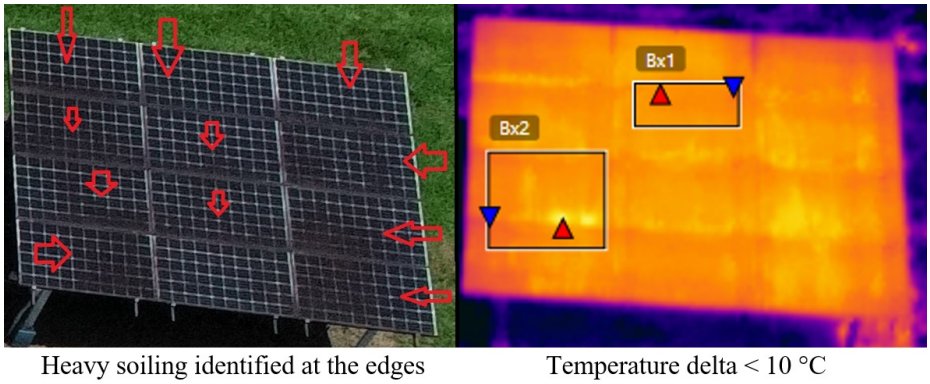

Fig. 11. RGB (left) and IR image (right) analyzed for experimental unit 2.

Figure 16 shows the summary of the failures detected with each of the techniques. It can be seen that VI identified more failures than IRT. The VI was able to detect all the failures, on the other hand, the IRT detected only 68% of the evaluated test, missing 45% of the cases of soiling.

The results of soiling failures for IRT are shown in the Fig. 17. IRT was not able to detect the 30 month natural soiling (S2). Also the types of soiling with

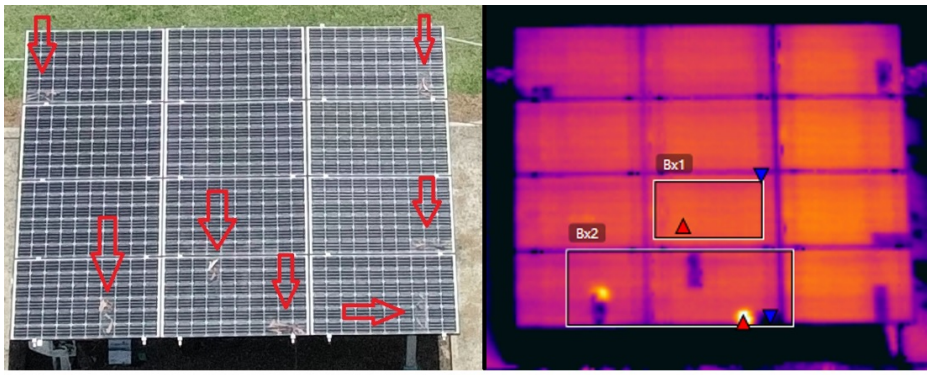

Fig. 12. RGB (left) and IR image (right) analyzed for experimental unit 6.

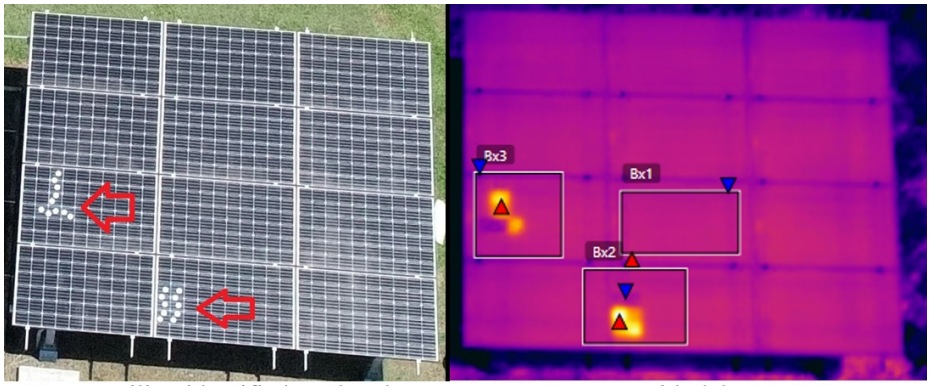

Fig. 13. RGB (left) and IR image (right) analyzed for experimental unit 18.

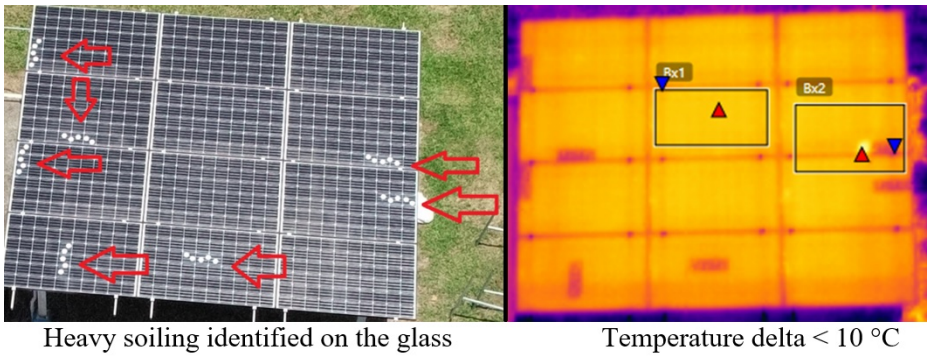

Fig. 14. RGB (left) and IR image (right) analyzed for experimental unit 19.

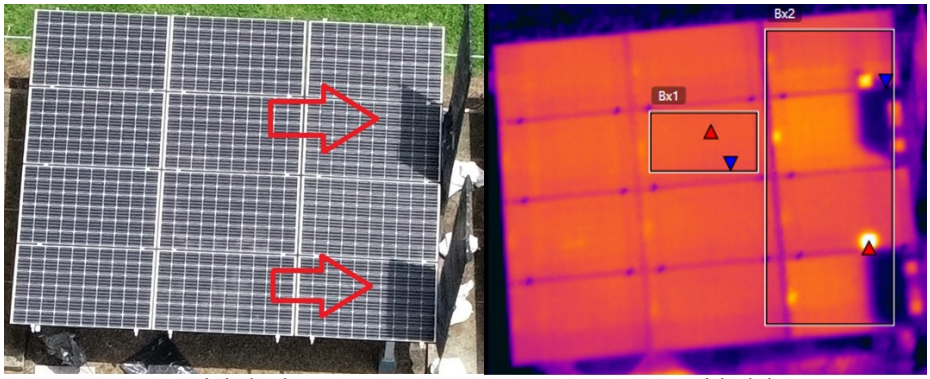

Fig. 15. RGB (left) and IR image (right) analyzed for experimental unit 22.

Table 8. Output variable of the experiment for IRT and VI. D = Detected, ND = Not detected

Experimental unit	Treatment	IRT output	VI output
1	S1	D	D
2	S2	ND	D
3	S1	D	D
4	S2	ND	D
5	S4	ND	D
6	S6	D	D
7	S4	D	D
8	S6	D	D
9	S4	D	D
10	S6	ND	D
11	S4	D	D
12	S6	D	D
13	S5	ND	D
14	S3	ND	D
15	S5	ND	D
16	S3	D	D
17	S5	D	D
18	S3	D	D
19	S5	ND	D
20	S3	ND	D
21	PS1	D	D
22	PS2	D	D
23	PS1	D	D
24	PS2	D	D
25	PS1	D	D
26	PS2	D	D
27	PS1	D	D
28	PS2	D	D

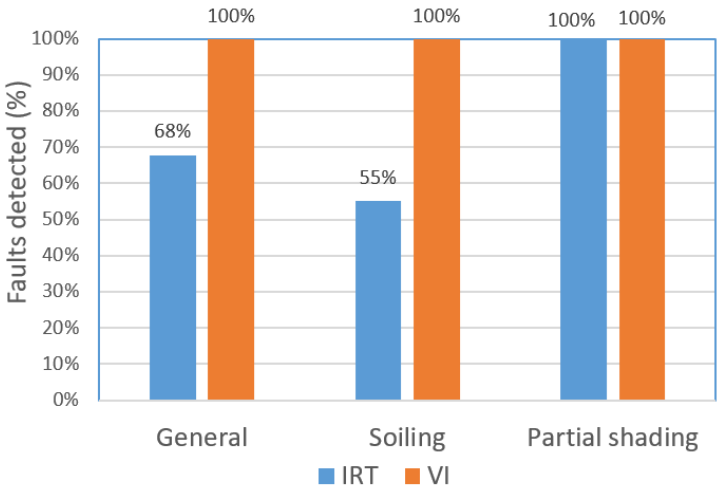

Fig. 16. Percentage of failures detected by each technique in the experiment.

white spots (S3 and S5) were the least detected. Finally, for the soiling with dry leaves (S4 and S6) there was one case of each that the failure could not be detected. Therefore, IRT is able to detect all types of soiling evaluated, however, there are levels of soiling that were not detected in some cases.

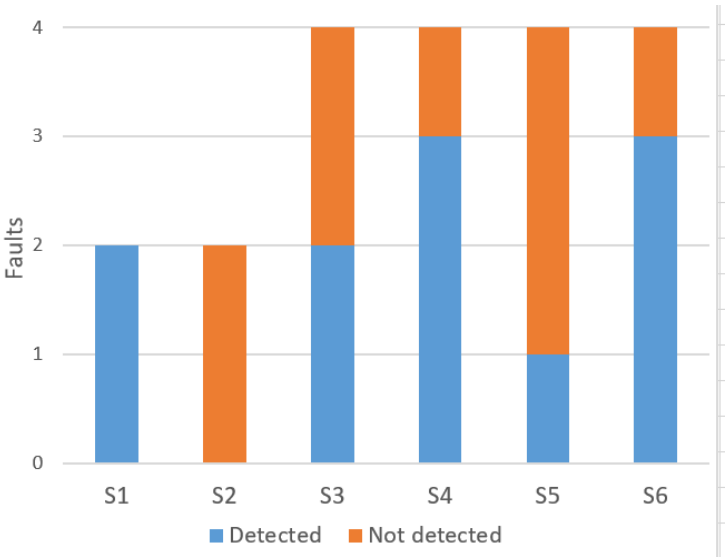

Fig. 17. Failures detected and not detected by the IRT under soiled conditions.

The detection of the failures was done strictly following the criteria of Table 5. However, in Fig. 11 it can be seen that through the IRT it was possible to appreciate a distortion in the thermal distribution of the PV array. In addition, in Fig. 14 it was possible to identify specific regions of lower temperature on the PV modules and temperature gradients lower than 10 °C, even though none of these cases met the requirement to be cataloged as failures, this suggests that, to detect soiling suboptimal conditions a lower threshold for the temperature gradient might be required.

4.2 Statistical analysis

To determine if one method performed significantly better than the other, a hypothesis test was done using Fisher's exact test [3, 19] as follows:

$$H_0 : N_i = N_j$$

$$H_a : N_i \neq N_j$$

$$\forall i \neq j$$

Where N is the number of identified failures, i and j are IRT and VI techniques respectively.

The test yields a p-value of p = 0.002 and odds ratio (OR) = 27.8, therefore, considering a significance level of $\alpha = 0.05$ it fulfills the alternative hypothesis ($p < \alpha$), i.e. significant differences were found between both methods [6]. In addition, when evaluating the hypothesis tests for each of the failure factors (soiling and partial shading) with the contingency tables shown in the Table 9, significant differences were obtained for soiling (S) with $p = 0.001$ and an OR = 33.87. The OR coefficient obtained in both cases indicate that there is a high probability that a fault will be not detect using IRT instead of VI, specifically detecting soiling [25]. That is, the VI is associated with a greater capacity for dirt detection compared to the IRT.

Table 9. Contingency table separating the factors (types of failures) of the experiment

Factor	**Technique**	**Result**		**Total**
		Not Detected	**Detected**	
S	TI	9	11	20
	VI	0	20	20
	Total	9	31	40
PS	TI	0	8	8
	VI	0	8	8
	Total	0	16	16
Total	TI	9	19	40
	VI	0	28	40
	Total	9	47	56

Another way to compare both methods is by the sensitivity in the effectiveness of fault detection, this is based on the analysis of true positives achieved by each technique [33]. The results show that IRT had a sensitivity of 68% while VI had 100%.

5 Conclusions

The present paper has analyzed two image-based fault detection technique (IRT and VI) for photovoltaic arrays for two of the most common temporary faults or suboptimal conditions, i.e., soiling and shading. Partial shadows were correctly detected with both techniques, however, IRT did not perform as well as VI for the detection of soiling. Nevertheless, IRT did detect at least once all the types of faults evaluated. The results also suggest that soling with IRT might be detectable if a temperature difference threshold smaller than 10 °C is used.

The methodology used allowed a quantitative comparison from experimental data between two techniques for failure detection in PV systems. This can be used for future experiments with other configurations of PV arrays and other types of failures, making it possible to validate theoretical models that are still being studied and to generate quantitative indicators of the effectiveness of each technique. Including treatments of conditions that are an apparent failure but without a significant affectation on power will allow studying the capacity of each technique to discriminate between true and false failures; this is pending for future research.

Acknowledgement

This paper is part of a project 5402-1360-4201 "Identificación de Fallas en Sistemas Fotovoltaicos" financed by the Costa Rica Institute of Technology. In addition, the first author is part of the Master of Science: Maestría en Ciencia y Tecnología para la Sostenibilidad of DOCINADE. Thanks to the Electronics students at TEC Dalberth Alberto Corrales Alpizar and Jose Eduardo Zuñiga Ramirez for their contribution in the development of the data acquisition system and John Martin Chacon Zambrana for the support in the data collection of the experiment.

References

1. Acciani, G., Falcone, O., Vergura, S.: Typical defects of PV-cells. IEEE International Symposium on Industrial Electronics pp. 2745–2749 (2010). https://doi.org/10.1109/ISIE.2010.5636901
2. Alsafasfeh, M., Abdel-Qader, I., Bazuin, B.: Fault detection in photovoltaic system using SLIC and thermal images. In: 2017 8th International Conference on Information Technology (ICIT). IEEE (may 2017). https://doi.org/10.1109/icitech.2017.8079925

3. Bolboacă, S.D., Jäntschi, L., Sestraş, A.F., Sestraş, R.E., Pamfil, D.C.: Pearson-fisher chi-square statistic revisited. Information **2**(3), 528–545 (sep 2011). https://doi.org/10.3390/info2030528
4. Cardinale-Villalobos, L., Rimolo-Donadio, R., Meza, C.: Solar panel failure detection by infrared uas digital photogrammetry: A case study. International Journal of Renewable Energy Research (IJRER) **10**(3), 1154–1164 (2020)
5. Chaudhary, A.S., Chaturvedi, D.: Thermal Image Analysis and Segmentation to Study Temperature Effects of Cement and Bird Deposition on Surface of Solar Panels. International Journal of Image, Graphics and Signal Processing **9**(12), 12–22 (2017). https://doi.org/10.5815/ijigsp.2017.12.02
6. Cohen, H.W.: P values: Use and misuse in medical literature. American Journal of Hypertension **24**(1), 18–23 (jan 2011). https://doi.org/10.1038/ajh.2010.205
7. Cubukcu, M., Akanalci, A.: Real-time inspection and determination methods of faults on photovoltaic power systems by thermal imaging in turkey. Renewable Energy **147**, 1231–1238 (mar 2020). https://doi.org/10.1016/j.renene.2019.09.075
8. Felipe-García, B., Hernández-López, D., Lerma, J.L.: Analysis of the ground sample distance on large photogrammetric surveys. Applied Geomatics **4**(4), 231–244 (2012). https://doi.org/10.1007/s12518-012-0084-2
9. FLIR: A guide to inspecting solar fields with thermal imaging drones (2019), https://thermalcapture.com/wp-content/uploads/2019/08/pv-system-inspection-thermal-drones-07-15-19.pdf
10. Flir: Flir Vue Pro and Flir Vue Pro R (2019), http://www.flir-vue-pro.com/wp-content/uploads/2016/10/FLIR-VUE-Pro-R-Datasheet-TeAx.pdf
11. Flir.com: Adjusting Sensitivity & Gain On The FLIR Vue Pro R (2019), https://flir.custhelp.com/app/answers/detail/a{_}id/3134
12. Gallardo-Saavedra, S., Hernandez-Callejo, L., Duque-Perez, O.: Image resolution influence in aerial thermographic inspections of photovoltaic plants. IEEE Transactions on Industrial Informatics **14**(12), 5678–5686 (dec 2018). https://doi.org/10.1109/tii.2018.2865403
13. Gutiérreza-Pulido, H., De la Vara-Salazar, R.: Análisis y diseño de experimentos. McGraw-Hill Interamericana, México D.F, second edn. (2008)
14. Hernández Sampieri, R., Fernández Collado, C., Baptista, L., Del Pilar, M.: Metodología de la investigación. Mc Graw Hill, México, fifth edn. (2010)
15. Higuchi, Y., Babasaki, T.: Failure detection of solar panels using thermographic images captured by drone. In: 2018 7th International Conference on Renewable Energy Research and Applications (ICRERA). IEEE (oct 2018). https://doi.org/10.1109/icrera.2018.8566833
16. International Energy Agency: Review of Failures of Photovoltaic Modules. Tech. Rep. July, Performance and Reliability of Photovoltaic Systems (2014)
17. International Energy Agency: Review on Infrared and Electroluminescence Imaging for PV Field Applications. Tech. rep., PHOTOVOLTAIC POWER SYSTEMS PROGRAMME (2018)
18. Javed, W., Wubulikasimu, Y., Figgis, B., Guo, B.: Characterization of dust accumulated on photovoltaic panels in doha, qatar. Solar Energy **142**, 123–135 (jan 2017). https://doi.org/10.1016/j.solener.2016.11.053
19. Jones, J.B., Schropp, M.A.: Research fundamentals: Statistical considerations in research design: A simple person's approach. Academic Emergency Medicine **7**(2), 194–199 (2000). https://doi.org/10.1111/j.1553-2712.2000.tb00529.x

20. Leva, S., Aghaei, M., Grimaccia, F.: PV power plant inspection by UAS: Correlation between altitude and detection of defects on PV modules. In: 2015 IEEE 15th International Conference on Environment and Electrical Engineering (EEEIC). IEEE (jun 2015). https://doi.org/10.1109/eeeic.2015.7165466
21. Linder, W.: Introduction. In: Digital Photogrammetry, chap. Introduction, pp. 10–12. Springer-Verlag Berlin, 4 edn. (2016). https://doi.org/10.1007/978-3-662-50463-5
22. M. Köntges: Reviewing the practicality and utility of electroluminescence and thermography (2014), https://www.nrel.gov/pv/assets/pdfs/2014{_}pvmrw{_}33{_}kontges.pdf
23. Madeti, S.R., Singh, S.: A comprehensive study on different types of faults and detection techniques for solar photovoltaic system. Solar Energy **158**, 161–185 (dec 2017). https://doi.org/10.1016/j.solener.2017.08.069
24. Maghami, M.R., Hizam, H., Gomes, C., Radzi, M.A., Rezadad, M.I., Hajighorbani, S.: Power loss due to soiling on solar panel: A review. Renewable and Sustainable Energy Reviews **59**, 1307–1316 (jun 2016). https://doi.org/10.1016/j.rser.2016.01.044
25. Mchugh, M.L.: The odds ratio: calculation, usage, and interpretation. Biochemia medica **19**(2), 120–126 (2009), https://hrcak.srce.hr/37593
26. Mekki, H., Mellit, A., Salhi, H.: Artificial neural network-based modelling and fault detection of partial shaded photovoltaic modules. Simulation Modelling Practice and Theory **67**, 1–13 (sep 2016). https://doi.org/10.1016/j.simpat.2016.05.005
27. Mellit, A., Tina, G., Kalogirou, S.: Fault detection and diagnosis methods for photovoltaic systems: A review. Renewable and Sustainable Energy Reviews **91**, 1–17 (aug 2018). https://doi.org/10.1016/j.rser.2018.03.062
28. Moretón, R., Lorenzo, E., Narvarte, L.: Experimental observations on hot-spots and derived acceptance/rejection criteria. Solar Energy **118**, 28–40 (aug 2015). https://doi.org/10.1016/j.solener.2015.05.009
29. Murillo-Soto, L., Meza, C.: Fault detection in solar arrays based on an efficiency threshold. In: 2020 IEEE 11th Latin American Symposium on Circuits Systems (LASCAS). pp. 1–4 (2020). https://doi.org/10.1109/LASCAS45839.2020.9069046
30. Murillo-Soto, L., Meza, C.: Photovoltaic array fault detection algorithm based on least significant difference test. In: Applied Computer Sciences in Engineering. WEA 2020. Communications in Computer and Information Science, vol. 1274. Springer-Verlag Berlin (2020). https://doi.org/10.1007/978-3-030-61834-6_43
31. Mäki, A., Valkealahti, S.: Power losses in long string and parallel-connected short strings of series-connected silicon-based photovoltaic modules due to partial shading conditions. IEEE Transactions on Energy Conversion **27**(1), 173–183 (mar 2012). https://doi.org/10.1109/tec.2011.2175928
32. National Renewable Energy Laboratory: Development of a Visual Inspection Data Collection Tool for Evaluation of Fielded PV Module Condition (2012). https://doi.org/10.2172/1050110, http://www.osti.gov/bridge
33. Pintea, S., Moldovan, R.: The Receiver-Operating Characteristic (ROC) analysis: Fundamentals and applications in clinical psychology. Journal of Cognitive and Behavioral Psychotherapies **9**(1), 49–66 (2009)
34. Sisodia, A.K., kumar Mathur, R.: Impact of bird dropping deposition on solar photovoltaic module performance: a systematic study in western rajasthan.

Environmental Science and Pollution Research **26**(30), 31119–31132 (aug 2019). https://doi.org/10.1007/s11356-019-06100-2
35. Tango, T.: Repeated Measures Design with Generalized Linear Mixed Models for Randomized Controlled Trials. Taylor & Francis Group, Tokyo Japan (2017)
36. Tsanakas, J.A., Ha, L., Buerhop, C.: Faults and infrared thermographic diagnosis in operating c-si photovoltaic modules: A review of research and future challenges. Renewable and Sustainable Energy Reviews **62**, 695–709 (sep 2016). https://doi.org/10.1016/j.rser.2016.04.079
37. Tyutyundzhiev, N., Lovchinov, K., Martínez-Moreno, F., Leloux, J., Narvarte, L.: Advanced PV modules inspection using multirotor UAV. In: 31st European Photovoltaic Solar Energy Conference and Exhibition. Hamburg (2015), https://www.researchgate.net/publication/283087341
38. Watson, J.J., Hudson, M.D.: Regional scale wind farm and solar farm suitability assessment using GIS-assisted multi-criteria evaluation. Landscape and Urban Planning **138**, 20–31 (jun 2015). https://doi.org/10.1016/j.landurbplan.2015.02.001
39. Wohlin, C., Runeson, P., Höst, M., Ohlsson, M.C., Regnell, B., Wesslén, A.: No Title. Springer, New York (2012). https://doi.org/10.1007/978-3-642-29044-2
40. Zefri, Y., ElKettani, A., Sebari, I., Lamallam, S.A.: Thermal infrared and visual inspection of photovoltaic installations by UAV photogrammetry—application case: Morocco. Drones **2**(4), 41 (nov 2018). https://doi.org/10.3390/drones2040041

Article 3.

Quantitative comparison of infrared thermography, visual inspection, and electrical analysis techniques on photovoltaic panels: a case study.

State: To be summited

Authors: Cardinale-Villalobos, L., Meza, C., Méndez-Porras, A. & Murillo-Soto, L. D

Year: 2021

Quantitative comparison of infrared thermography, visual inspection, and electrical analysis techniques on photovoltaic panels: a case study

Leonardo Cardinale-Villalobos[1][0000−0002−9649−6017], Carlos Meza[1][0000−0002−7374−505X], Abel Méndez-Porras[2][0000−0001−8038−7839], and Luis D. Murillo-Soto[3][0000−0002−6601−1082]

[1] Electronics Engineering School, Instituto Tecnológico de Costa Rica, Costa Rica
lcardinale@tec.ac.cr
[2] Computer Engineering Department, Instituto Tecnológico de Costa Rica, Costa Rica
[3] Electromechanic Engineering School, Instituto Tecnológico de Costa Rica, Costa Rica

Abstract. Solar farms are exposed to failures that cause a decrease in performance. Infrared thermography (IRT), visual inspection (VI) and electrical analysis (EA) are examples of methods to deal with faults. In order to make the best use of the PV installation, it is necessary to make optimal use of failure detection techniques, however, there is a lack of information about the effectiveness of each method to achieve this. This article calculates and compares the effectiveness of VI, IRT and EA in detecting soiling, partial shadows and electrical faults by applying an experiment in a real PV system using low-cost equipment. The results showed that there were no significant differences in the number of failures detected by the three techniques, however, the visual inspection was the best at detecting soiling and the worst at detecting electrical failures, in addition, the partial shadows were the type of failure that was most detected by all the techniques. The results contribute to a better use of PV systems, through objective information for the correct selection of failure detection methods.

Keywords: Solar PV System · Fault detection performance · Partial shading · Soiling · electrical faults · Thermography · electrical analysis

1 Introduction

The benefit of PV systems is determined by their performance over their lifetime. Due to electrical failures, partial shading and soiling, the power delivered by the solar panels decreases and may even generate irreversible damage [Zhao, 2015]. Therefore, it is critical to be able to effectively detect these conditions.

By using infrared thermography [Zefri et al., 2018], visual inspection [Madeti and Singh, 2017] and electrical analysis [Murillo-Soto and Meza, 2020], it is

possible to detect failures to act in a timely manner before a major impact on the energy delivered [Zhao, 2015] or a fire occurs [Mellit et al., 2018], These have contributed to the better performance of the system over time [Madeti and Singh, 2017] and to fire prevention [Mellit et al., 2018]. Although these techniques have been widely used, there is a lack of quantitative information [Appiah et al., 2019] that allows us to know their effectiveness in detecting failures, therefore, it is not possible to give optimal maintenance to PV systems through a correct selection of failure detection methods. To contribute to the solution of the problem, as a previous stage to this research, a methodology was proposed to compare the effectiveness for failure detection of infrared thermography and visual inspection [Cardinale-Villalobos et al., 2020b].

In this research an experiment was developed replicating the methodology and experiment proposed by [Cardinale-Villalobos et al., 2020b]. In this way, it was compared the effectiveness of IRT, VI and EA to detect failures by shading, soiling and electrical faults. The rest of the paper is structured as follows: firts the suboptimal conditions considered are described, then the material and methods are presented. Section 4 presents the main results and section 5 gathers the main conclusions.

This research contributes to the characterization of failure detection methods from the generation of quantitative indicators that have been absent. This contributes to a better selection of failure detection methods, and also allows identifying the strengths and limitations of each method in the face of specific failures, which can be used to improve each failure detection technique.

2 Suboptimal conditions considered

For the comparative analysis we consider the following suboptimal conditions:

- Partial shadowing: A partial shadow on a PV array creates a specific region in which the irradiance is lower, resulting in a decrease in the power of the entire array [Mellit et al., 2018]. Figure 1 shows a PV array with a shaded region due to a tree on the left, and dirt on the panel on the right. Both cases cause a decrease in power, which will depend on the size and degree of shading [Mäki and Valkealahti, 2012, Maghami et al., 2016].

- Soiling: The presence of dust, leaves, dirt and generally any kind of dirt will cause a decrease in the power generated by a solar array, which will be greater as the amount of dirt increases [Maghami et al., 2016]. Uniform dirt (evenly distributed dust) [Javed et al., 2017] and non-uniform dirt (patches of dirt or bird drops) will have an affection on the power; the latter can also be classified as shading, since it creates a decrease in the irradiance that affects the PV panel, equivalent to a partial shade. The effect on the power due to non-uniform dirt causes a hot spot to be formed [Maghami et al., 2016]. Figure 2 shows a PV array with natural dirt, in which, non-uniform dirt can be observed.

– Electrical Faults: From the electrical point of view, the failures can be classified as follows 1) Ground faults, 2) Interline faults, 3) Open circuit faults, 4) others. [Zhao, 2015]. Faults cause a decrease in the power delivered and an increase in the temperature that varies according to the type of fault [Appiah et al., 2019, Chaudhary et al., 2018, Tsanakas et al., 2016, Wang et al., 2016]. In this investigation, the following faults were applied: short circuit in a panel, ground fault, and open circuit. These are represented in Fig. 3 with red lines.

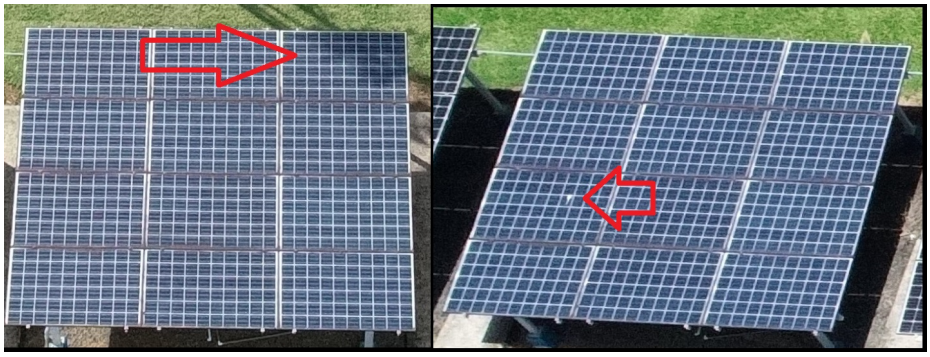

Fig. 1. PV-chain of the analysed installation, with partial shade due to a tree (left) and dirt due to a foreign object (right).

Fig. 2. Monocrystalline PV module analyzed with the presence of natural non-uniform dirt.

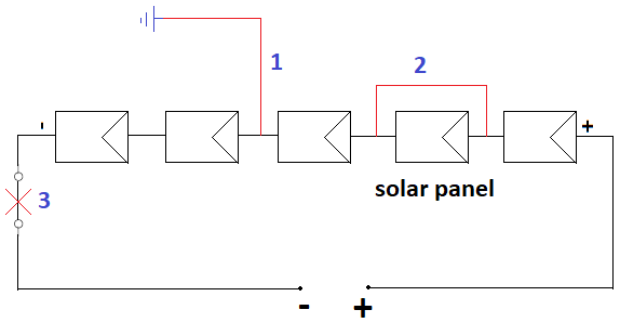

Fig. 3. Types of solar panel failures analyzed in this research. 1) Short circuit to ground, 2) Short circuit in panel and 3) Open circuit.

3 Materials and methods

As it was mentioned before, it was replicated the methodology proposed by [Cardinale-Villalobos et al., 2020a], in order to analyze the effectiveness of a failure detection method for the analysis of electric variables. Moreover, the results were used to compare VI, IRT and EA techniques in case of soiling, shading and electric faults. The methodology is detailed in the following sections.

3.1 The PV installation analyzed

The photovoltaic installation used for this research has a ground mount and is located at the San Carlos Local Technological Campus in Santa Clara, Costa Rica. It is made up of six PV arrays, of which, three of monocrystalline technology were used for the development of the experiment because the EA method is designed for monocrystalline modules. The details of the PV arrays used are shown in the Table 1.

Table 1. Information about the PV arrays analyzed

Longitude	-84.51
Latitude	10.36
Azimut angle	0° with respect to the South
Inclination angle	15°
Peak DC power (kW)	3.36
Number of PV panels	12
PV panel models	Canadian Solar CS6k-280M
Total surface (m^2)	19.6
Date of commissioning	May 31st, 2017

The installation used in the research consists of 6 PV arrays of 12 monocrystalline and polycrystalline modules in series, each connected to a Sunny Boy 3000TL-US SMA inverter. The monocrystalline arrays selected as test subjects in this research are identified by the numbers 2, 4 and 6 in the Fig. 4.

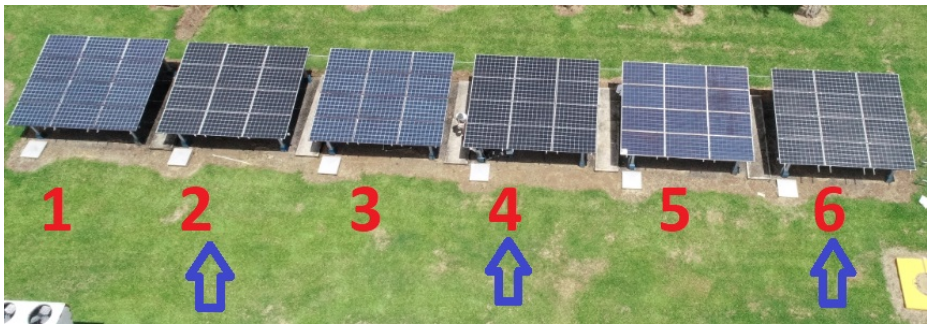

Fig. 4. Aerial photo of the analyzed PV installation. The monocrystalline strings 2, 4 and 6 were used in this research.

3.2 Instrumentation

For the development of the experiment, a drone and a series of instruments were used as detailed in Fig. 6. Each one is detailed below:

- Drone Phanton 4 Pro with a FLIR VUE PRO R thermal camera. The specifications of the RGB camera are shown in Table 2 and those of the thermal camera in Table 3.
- Vantage Pro2 Weather Station with temperature sensor to measure the ambient temperature required for thermogram analysis. Accuracy is 0.3 °C.
- Spektron 2010 pylanometer to verify that minimum irradiance conditions are met and to apply the EA method. The accuracy is ± 5% of the annual measurement.
- Invert for the measurement of real power required by the AI. Accuracy meets ANSI C12.20 standard.
- Digital contact temperature sensor model DS18B20 to apply the AI. Accuracy is ± 0.5 °C.

3.3 Experiments

An experiment was developed by inducing the faults of interest and the three fault detection techniques were applied to each one.

The experiment used a repeated measurement design because multiple treatments had to be applied to the same subjects [Tango, 2017]. A total of 40 experimental units were analyzed from the 11 treatments applied to the 2 subjects

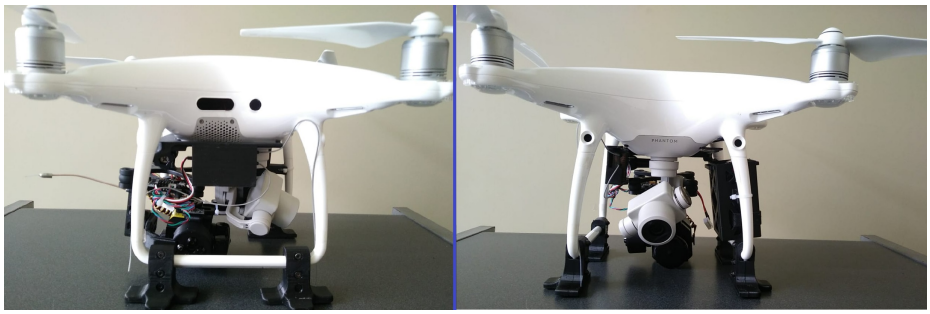

Fig. 5. Side (left) and front (right) view of the drone with infrared and RGB cameras used in the investigation.

Table 2. Characteristics of the RGB camera used

Parameter	**Value**
Sensor	1" CMOS/ Effective pixels 20M
Lens	FOV 84° 8.8 mm/24mm
PIV Image Size	4096 x 2160
Photo	JPEG
Image Size	3:2, 4:3, 16:9
ISO Range	100-3200 (Auto)

Table 3. Characteristics of the FLIR VUE PRO R 336 thermal camera [Flir.com, 2019, Flir, 2019]

Parameter	**Value**
HFOV x VFOV	25°x 19°
Sensor (width x height)	5.764 mm x 4.351 mm
Focal length	13.00 mm
Image width x height	336 x 256
Frequency	9 Hz
Accuracy	+/- 5 °C o 5% from reading
Thermal sensitivity	40 mK
Sensor	Uncooled microbolometer

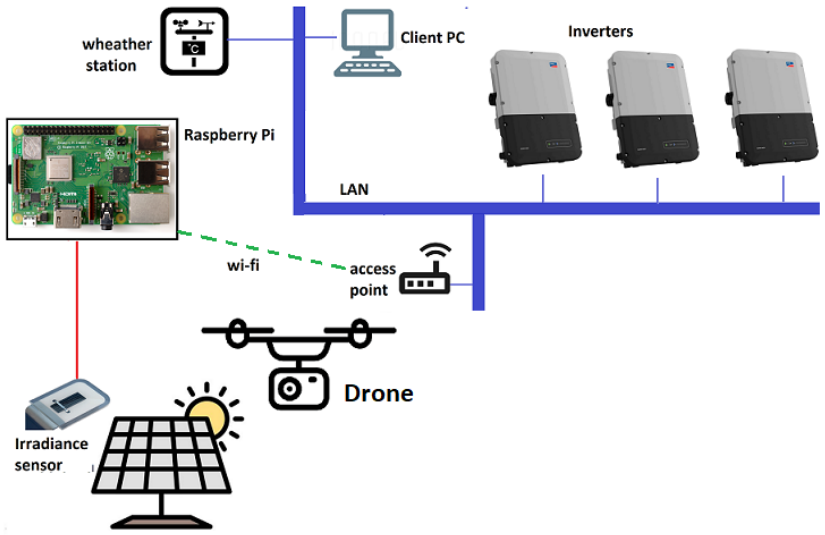

Fig. 6. Schematic diagram of the communication links used to access the information sources of the experiment.

(Strings 4 and 6). String 2 was used as a control subject to establish a reference condition in each experimental unit for the normal operation of the PV strings, i.e. without applying failures. The factors and levels evaluated are shown in Table 4.

The treatments were applied to the subjects without interaction between factors. Each level was applied in both subjects making two repetitions in each one (Except S1 and S2, which were each applied to a single test subject because it was natural soiling). The selection of the modules of each string to which the failure was applied was chosen at random. It was assumed that there is an independent relationship between the treatments, because they were randomized and do not generate a residual effect in the subject [Gutiérreza-Pulido and De la Vara-Salazar, 2008], i.e., the PV string return to their normal state once the treatment is removed. Each of the treatments is described in the following section.

3.4 Description of each factor and the levels of the experiment

The soiling and partial shading treatments developed in [Cardinale-Villalobos et al., 2020a] were replicated and the treatments corresponding to electrical failures were included. Each is described in this section.

– **A. Soiling**

Six soiling treatments were used; these are identified as S1-S6 in table 4. For the treatments S3 and S5, the glasses shown in Fig. 7) were used. For the

Table 4. Factors (types of failures) and levels used to generate the diverse treatments to be evaluated in the experiment.

Treatment	Factor	Level
S1	Soiling	10 months of natural soil
S2		30 months of natural soil
S3		12 cells with white spots
S4		12 cells with dry leaves from the site
S5		21 cells with white spots
S6		21 cells with dry leaves from the site
PS1	Partial shading	Shading of approximately 70% of a panel's area
PS2		2 shadows, each approximately 30% of the area of a panel
E1	Electrical fault	Short circuit in module
E2		Ground fault in second module
E3		Open circuit in the array

treatments S4 and S6 the glasses shown in Fig. 8 were used. The glasses used were 480mm x 160mm x 5mm.

The treatments S3 and S5 were prepared by applying white paint to the glass. Treatments S4 and S6 used leaves and seeds found on site around the solar panels. These treatments represent failures due to strong shading [Maghami et al., 2016].

Fig. 7. Glass with white circles used to simulate dirt obstructing the path of radiation in three PV cells.

– **B. Partial shading**

The PS1 and PS2 treatments generated a natural shade allowing the incidence of diffuse radiation [Mekki et al., 2016]. For this, an object was placed next to the PV array (see Fig. 9) at 9:30 am for PS1 and at 10:30 am for PS2.

– **C. Electrical faults**
In previous research work, electrical failures were evaluated at the experimental level by modifying the electrical connections of the PV system, e.g. open circuits and short circuits [Zhao et al., 2013]. Using this as a reference, switches were installed in the study PV arrays to emulated that effect; an

Fig. 8. Glass with dry leaves and seeds to simulate dirt obstructing the radiation path in three PV cells.

Fig. 9. Object used to generate the treatments of partial shade failures. The shadow generated corresponds to the PS1 treatment.

electrical diagram of how this was implemented is shown in Fig 10. The E1 treatment was randomly located in each of the experimental units evaluated. E2 was applied maintaining the fixed position to generate a short circuit at a low voltage and not to expose the circuit to electric arcs. The E3 treatment has the same effect in any location due to the series circuit configuration of all the modules, therefore, the location of the switch was not changed.

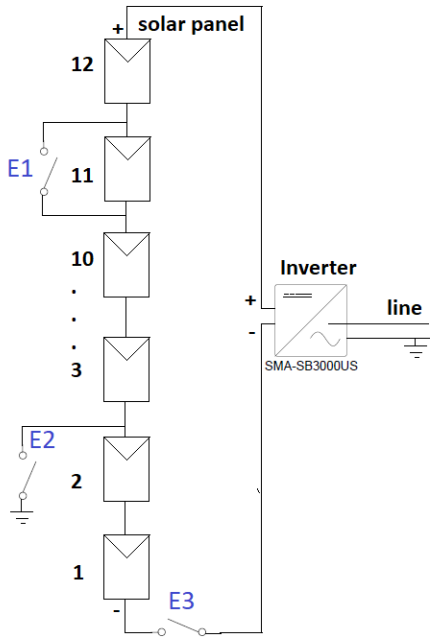

Fig. 10. Diagram of the location of the switches used to generate the electrical failure treatments evaluated in the experiment.

3.5 Protocol for IRT and VI missions

The protocol used in [Cardinale-Villalobos et al., 2020b] was replicated. For each treatment, a flight was made with the UAS capturing RGB and infrared images of the PV chains. The flight height was 25 m to detect possible failures with a PV cell resolution [Cardinale-Villalobos et al., 2020b] for IRT and VI. The irradiance was always higher than 700 W/m2 with an angle around 20° from the panel perpendicular, the sky was clear and there were no wind currents. Emissivity was 0.85 for IRT. Consecutive images were taken every 1 s for the IRT and 2 s for the VI. The thermal images were configured to contain the radiometric information in RJPEG format.

For each test, the irradiance, ambient temperature and relative humidity were recorded. Each treatment was applied 15 minutes before the measurement was taken to ensure that thermal equilibrium existed [International Energy Agency, 2018].

3.6 Protocol for EA measurements

This method was based on the comparison between the real generated power and the estimated theoretical power. The model used to estimate the generated power is the one proposed by [Murillo-Soto and Meza, 2020]; see (1).

$$\eta_T(T,G) = -765.231E-6 \cdot T + 7.484E-06 \cdot G + 182.712E-3$$

(1)

For greater accuracy in the model, wiring and aging losses were included as shown below:

$$\eta_l(T,G) = \eta_T(T,G)(1-l_w)(1-l_y)$$

(2)

Where, $l_w = 0.01$ and represents the electrical wiring losses and $l_y = 0.03625$ represents the aging losses according to the manufacturer's information. Finally, the system was tested under normal conditions to be empirically calibrated using the control subject (string 2), so a correction factor k was applied and a constant a was added to obtain the equation used by the EA method:

$$\eta_E(T,G) = 1.0111\eta_E - 35.734)$$

(3)

When applying each treatment, it was waited at least 5 minutes to take the measurements of the required physical variables, ensuring that the measurement corresponded to the steady state of the failure. In order to establish this parameter, it was considered that in case of a variation in the PV array conditions (e.g., a failure), the inverter takes a time to reach the stability of the new operation point [Pradhan and Panda, 2020], although this time can be less than 1 s, it was decided to leave a longer time.

Each measurement was obtained from the average of 1 min, this in order to have a measurement that was not affected by external fluctuations, namely: a) sudden changes in weather conditions and b) difference between the sampling times of the real power and the variables to estimate the theoretical power.

3.7 Fault detection criteria

The IRT was based on the analysis of the images in search of hot spots using the criteria indicated by [Moretón et al., 2015, International Energy Agency, 2014].

The VI considered the guide presented by [National Renewable Energy Laboratory, 2012].

For the EA method, the literature review showed that there is no single criterion that defines how much power loss can be considered a failure. For this research we used the criteria proposed by [Acciani et al., 2010], which indicates that a failure exists when the power falls by at least 4%.

Table 5 details the fault detection criteria used in the experiment.

Table 5. Criteria used for each technique evaluated to detect the failures induced from each treatment

Technique	Criteria for fault detection
IRT	Hot spot with a delta $\geq$ 10 °C
	PV-chain with a temperature delta 3.5 C in relation to a neighboring chain
VI	Presence of radiation attenuation on the panel due to shade
	Appearance of light or heavy soiling
	Burned marks or discoloration
EA	Reduction of 4% or more compared to the theoretical power

3.8 Date and conditions of the experiment

The IRT and VI measurements were made between august 18th and september 2nd, 2020. EA measurements were made between September 17th and October 30th. The average ambient temperature was 30 °C, the relative humidity 60% and the reflected temperature 22 °C.

3.9 Power normalizing

A comparison was made of the average power generated between the study subjects (strings 4 and 6) and the control subject (string 2). The measurement was made during two hours with an irradiance greater than 700 W/m^2. A difference of 0.67% and -0.59% was obtained for strings 4 and 6 respectively. These results allowed to consider that the strings are equivalent.

4 Results and discussion

4.1 Power affect for each experimental unit

Each treatment was applied to the study subjects (strings 4 and 6) and was compared with the control subject (string 2), with this, it was verified that all the experimental units had an affectation of at least 4% [Acciani et al., 2010], ie, that it met the criteria of failure. The results are shown in Table 6, these considered the effect of power normalization calculated in section 3.9.

4.2 Results of the experiment

For each experimental unit, a discrete output variable was generated to indicate whether or not the technique detected failure; the results are shown in Table 7. The results of the IRT and VI in the presence of soiling and partial shading failures were taken from [Cardinale-Villalobos et al., 2020a].

Table 6. Validation of the effect on power of each of the treatments evaluated in the experiment

Experimental unit	Irradiance W/m^2	Reference array power (W)	Tested array power (W)	Power reduction	Fault (Yes/no)
1	783	2148	1885	12%	Yes
2	783	2148	1472	31%	Yes
3	724	2126	1872	12%	Yes
4	724	2126	1449	32%	Yes
5	775	2528	1876	26%	Yes
6	887	2883	1915	34%	Yes
7	836	2671	2150	20%	Yes
8	1040	3421	2541	26%	Yes
9	984	3086	2593	16%	Yes
10	943	3077	2066	33%	Yes
11	1059	3285	2884	12%	Yes
12	956	3201	2141	33%	Yes
13	971	3197	2611	18%	Yes
14	866	2911	2215	24%	Yes
15	873	2897	2399	17%	Yes
16	944	3077	2288	26%	Yes
17	890	2839	2366	17%	Yes
18	868	2841	2370	17%	Yes
19	1041	3416	2892	15%	Yes
20	793	2533	2091	17%	Yes
21	782	2589	2148	61%	Yes
22	958	2662	1889	34%	Yes
23	887	2582	2146	61%	Yes
24	1035	3045	2586	26%	Yes
25	782	2601	246	18%	Yes
26	892	2870	721	75%	Yes
27	887	2582	2127	18%	Yes
28	1079	2890	2207	24%	Yes
29	1030	2904	0	100%	Yes
30	1238	3226	0	100%	Yes
31	1030	2904	0	100%	Yes
32	1033	2814	0	100%	Yes
33	907	2637	2435	7%	Yes
34	949	2662	2458	8%	Yes
35	1053	2832	0	100%	Yes
36	996	2622	0	100%	Yes
37	906	2637	2348	8%	Yes
38	949	2662	2446	11%	Yes
39	1027	2743	0	100%	Yes
40	998	2637	0	100%	Yes

4.3 Image analysis

Each experimental unit was analyzed manually for IRT and VI. The thermographs were processed with Flir Tools 5.13 and the RGB images were analyzed with traditional photo viewing software. Figures 11, 12 and 13 show some electrical failures analyzed with IRT. By means of the VI it was not possible to detect electrical failures.

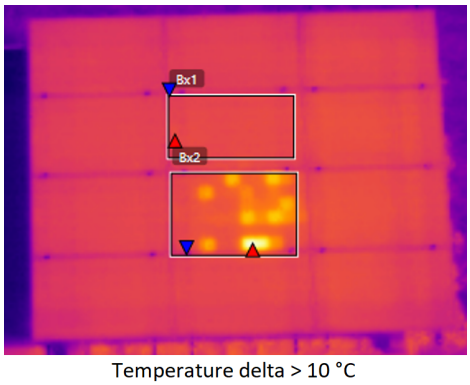

Fig. 11. IR image analyzed for the experimental unit 37. In this one, the heating generated in a solar panel due to the presence of a short circuit is observed.

4.4 EA analysis

Table 8 shows the detail of the measurements with the EA. It is observed that for all types of failures, in some experimental units the failure was not detected, this is due to the fact that the estimated power was less than it should be under conditions without failure (experimental units 18, 21 and 33). Also, cases were found in which the estimated power affect deviated by less than 1% from the criteria for detecting failure (experimental units 13, 19, 20 and 34); which shows that accuracy errors of less than 1% will affect the effectiveness of the technique. This requires high precision in the instrumentation, in the parameters of the mathematical model and in the processing of the information; with their respective experimental validation.

4.5 Comparison of the three techniques

A summary of the number of faults detected by each technique during the experiment is shown in Fig. 14. It can be observed that IRT was the technique that detected the most number of failures (78%), while VI was the one that detected

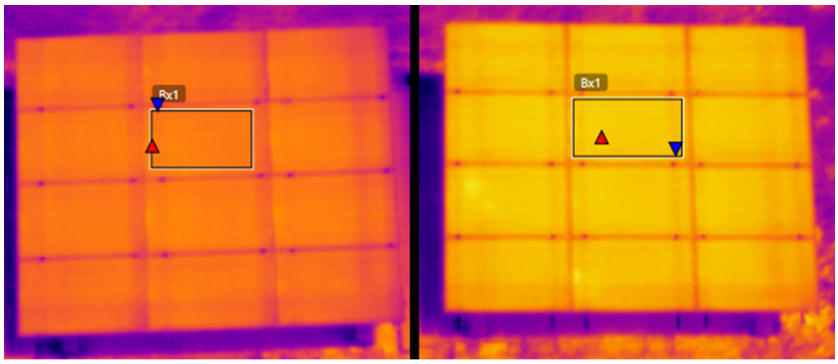

Fig. 12. IR images analyzed for experimental unit 39. String 2 (left) and string 6 (right). In this one, it can be seen that string 6 had a higher temperature than the control subject (string 2) due to the open circuit.

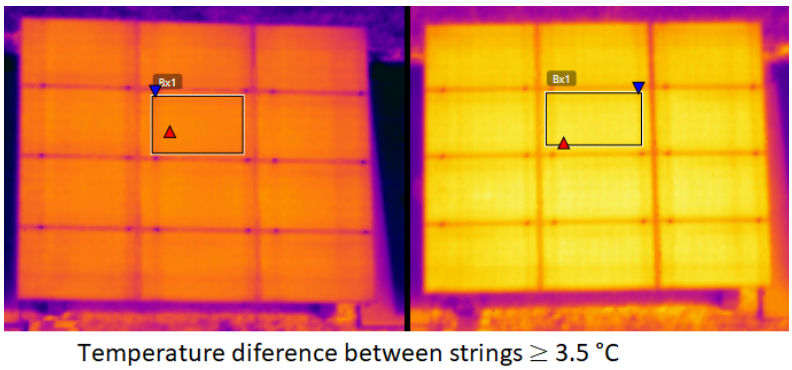

Fig. 13. IR images analyzed for experimental unit 30. String 2 (left) and string 4 (right). In this case, the short circuit to earth caused the inverter to open the circuit (electrical protection), causing an increase in the temperature of the entire string.

Table 7. Summary of the results of the experimen. D = Detected, ND = Not detected, S = soiling, PS = partial shading and E = electrical fault.

Experimental unit	**Factor**	**Treatment**	**IRT result**	**VI result**	**EA result**
1	S	S1	D	D	D
2	S	S2	ND	D	D
3	S	S1	D	D	D
4	S	S2	ND	D	D
5	S	S4	ND	D	D
6	S	S6	D	D	D
7	S	S4	D	D	ND
8	S	S6	D	D	D
9	S	S4	D	D	ND
10	S	S6	ND	D	D
11	S	S4	D	D	ND
12	S	S6	D	D	D
13	S	S5	ND	D	D
14	S	S3	ND	D	D
15	S	S5	ND	D	ND
16	S	S3	D	D	D
17	S	S5	D	D	ND
18	S	S3	D	D	ND
19	S	S5	ND	D	ND
20	S	S3	ND	D	ND
21	PS	PS1	D	D	ND
22	PS	PS2	D	D	D
23	PS	PS1	D	D	D
24	PS	PS2	D	D	D
25	PS	PS1	D	D	D
26	PS	PS2	D	D	D
27	PS	PS1	D	D	D
28	PS	PS2	D	D	D
29	E	E2	D	ND	D
30	E	E2	D	ND	D
31	E	E2	D	ND	D
32	E	E2	D	ND	D
33	E	E1	D	ND	ND
34	E	E1	D	ND	D
35	E	E3	D	ND	D
36	E	E3	D	ND	D
37	E	E1	D	ND	ND
38	E	E1	D	ND	D
39	E	E3	D	ND	D
40	E	E3	D	ND	D

Table 8. Electrical measurements for the evaluation of each treatment with the EA technique. The last column on the right indicates the output variable of this method

Experimental unit	**Irradiance (W/m2)**	**Tested array average temperature (°C)**	**Tested array power (W)**	**Estimated power (W)**	**Power reduction**	Fault (Yes/no)
1	783	50,4	1885	2191	14.0%	Yes
2	783	52,5	1472	2167	32.1%	Yes
3	724	50,5	1872	2015	7.1%	Yes
4	724	52,3	1449	1996	27.4%	Yes
5	775	56,9	1876	2092	10.3%	Yes
6	887	57,5	1915	2407	20.5%	Yes
7	836	57,8	2236	2258	1.0%	No
8	1040	53,6	2541	2910	12.7%	Yes
9	984	59,0	2593	2668	2.8%	No
10	943	49,0	2066	2686	23.1%	Yes
11	1059	57,1	2884	2914	1.0%	No
12	956	51,0	2141	2697	20.6%	Yes
13	971	52,0	2611	2728	4.3%	Yes
14	866	49,1	2215	2454	9.7%	Yes
15	873	53,0	2399	2424	1.0%	No
16	944	48,9	2288	2688	14.9%	Yes
17	890	57,0	2366	2423	2.3%	No
18	868	58,5	2370	2339	-1.3%	No
19	1041	48,9	2892	2985	3.1%	No
20	793	55,5	2091	2163	3.3%	No
21	782	56,5	2148	2118	-1.4%	No
22	958	60,3	1889	2574	26.6%	Yes
23	887	55,1	2146	2437	12.0%	Yes
24	1035	59,4	2664	2808	5.1%	Yes
25	782	57,8	246	2102	88.3%	Yes
26	892	54,0	721	2468	70.8%	Yes
27	887	54,2	2127	2449	13.2%	Yes
28	1079	56,6	2207	2980	26.0%	Yes
29	1030	55,0	0	2858	100.0%	Yes
30	1238	59,0	0	3408	100.0%	Yes
31	1030	57,0	0	2828	100.0%	Yes
32	1033	58,0	0	2822	100.0%	Yes
33	907	62,8	2435	2396	-1.6%	No
34	949	58,2	2458	2578	4.7%	Yes
35	1053	56,0	0	2913	100.0%	Yes
36	996	57,0	0	2730	100.0%	Yes
37	906	63,2	2348	2388	1.7%	No
38	949	54,7	2446	2626	6.9%	Yes
39	1027	56,0	0	2837	100.0%	Yes
40	998	55,0	0	2765	100.0%	Yes

Cases that were at 1% or less of the limit defined as criteria for failure detection are identified in light blue. Cases that showed an increase in power in the presence of the fault were marked in green

the least number (70%). These results vary from those found by [Cardinale-Villalobos et al., 2020a], in which VI detected more failures than IRT. Therefore, the design of the experiment will be closely related to the effectiveness found.

Analyzing the results for each type of failure: a) partial shading was mostly detected by all techniques (more than 88% in all three techniques), b) Soiling was detected to a minor extent by both IRT (55%) and EA (60%), and c) VI was most effective detecting soiling (100%) and shading (100%) but did not detect any electrical failure.

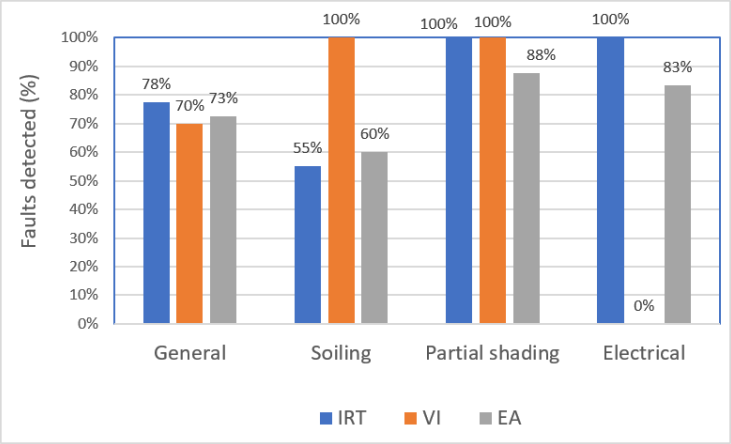

Fig. 14. Overall percentage and divided by type of failure for each treatment according to the results of the experimen.

Considering the output variable of continuous type (1 = detected and 0 = not detected), an analysis of the variance was made (see Fig.15). The variances were 0.191, 0 and 0.229 for soiling, partial shading and electrical faults respectively. This indicates that the detection of soiling and electrical faults had greater variability than those of partial shadows. The high variability detecting electrical faults is due to the fact that none of the faults generated burns or discoloration on the solar panel, however, the variability detecting soiling indicates that more research should be done focused on improving the effectiveness of IRT and EA detecting soiling.

Figure 16 shows the results of soiling detection by EA, in which, it can be seen that, all types of soiling were detected at least in a low percentage of occasions. This indicates that the EA technique do detect the types of soiling evaluated but with less effectiveness. The reasons why, in some cases this type of failure was detected and in others not, requires a more detailed study specifically on this subject. This compartment had also been identified for IRT detecting soiling [Cardinale-Villalobos et al., 2020a].

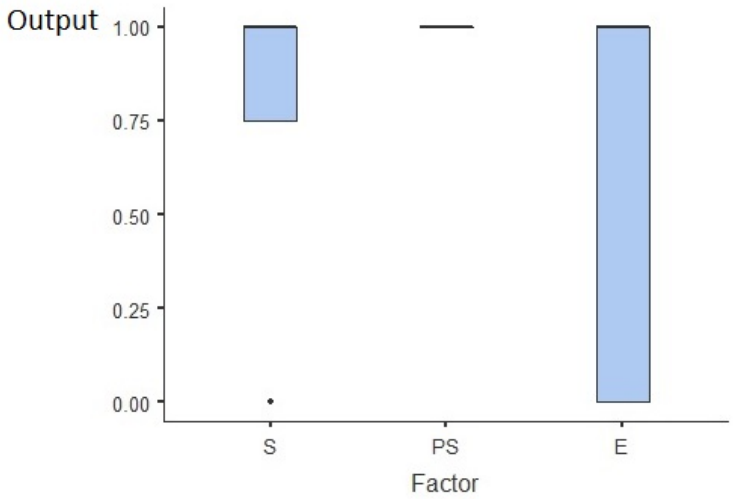

Fig. 15. The blue box represents the measurements obtained between quartiles Q1 and Q3

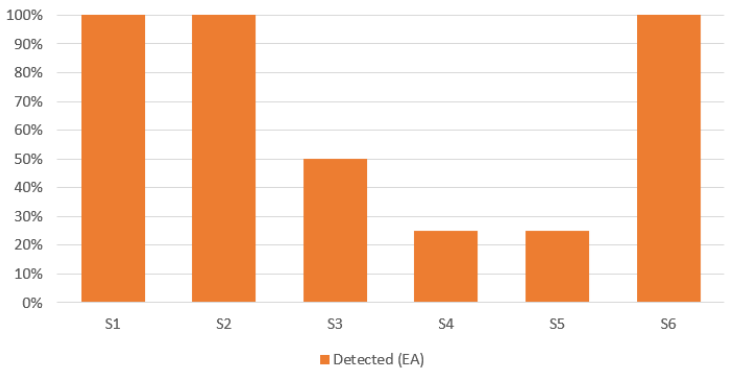

Fig. 16. Percentage of soiling failures that were detected by the EA. S1 and S2 were applied twice, the other four times.

The only technique that was based on qualitative criteria for the detection of failures was the VI, this implies that its effectiveness could be affected due to the subjectivity that could exist before other types of failures. The definition of quantitative criteria for the VI is an area that could vary the performance of the technique for certain types of failures.

4.6 Statistical hypothesis testing

Using contingency tables and Fisher's exact test, the effectiveness of the techniques can be evaluated by comparing them in pairs [Jones and Schropp, 2000, Bolboacă et al., 2011]. To determine if there is a significant difference between the total number of failures detected by each technique, the following hypothesis tests were defined: as follows:

$$H_{0,1} : N_i = N_j$$

$$H_{a,1} : N_i \neq N_j$$

$$H_{0,2} : N_i = N_k$$

$$H_{a,2} : N_i \neq N_k$$

$$H_{0,3} : N_j = N_k$$

$$H_{a,3} : N_j \neq N_k$$

$$\forall i \neq j \neq k$$

Where N is the number of identified failures, i, j and k are IRT, VI and EA techniques respectively. Table 9 shows the p-values obtained for each hypothesis test.

Table 9. P-value obtained for each of the hypotheses evaluated

Hypothesis	**p-value**
H01	0.446
H02	0.797
H03	1

.

Considering a significance level $\alpha = 0.05$ because no major requirement has been identified [Ventura-León, 2017], the three null hypotheses $H_{0,1}$, $H_{0,2}$ and $H_{0,3}$ are accepted, that is, statistically no significant differences were found in the number of failures detected between techniques. Each of the techniques was also compared for the different types of failure applied, for which p-value $< \alpha$ and odd ratio (OR) was obtained for the cases shown in Table 10.

From the analysis of Table 12 and Table 10, it was interpreted which method was better than another for each type of failure; this is summarized in Table 11. The OR coefficients shown indicate that, in addition to accepting the alternative hypotheses for these types of failure, there is a high probability that the technique will succeed in detecting a failure of this type compared to the other technique [Mchugh, 2009].

Table 10. P-value less than α and OR obtained by analyzing significant differences for each type of failure

Technique 1 – Technique 2	Type of fault	p-value	OR
EA-VI	S	0.003	27.80
EA-VI	E	<0.001	105*
IRT-VI	S	<0.001	33.87*
IRT-VI	E	<0.001	625

*The order of the column in the contingency table was changed to achieve OR >1

Table 11. Significant differences in the detection of each type of failure between the methods studied. Note: The types of failures not indicated had no significant differences.

Techniques	Result
EA-VI	VI detects soiling better
	EA detects electrical faults better
IRT-VI	VI detects soiling better
	IRT detects electrical faults better
IRT- EA	No significant differences were found

Table 12. Contingency table separating the factors (types of failures) of the experiment

Factor	Technique	Detected	Not Detected	Total
S	IRT	11	9	20
	VI	20	0	20
	EA	12	8	20
	Total	43	17	60
PS	IRT	8	0	8
	VI	8	0	8
	EA	7	1	8
	Total	23	1	24
E	IRT	12	0	12
	VI	0	12	12
	EA	10	2	12
	Total	22	14	36
Total	IRT	31	9	40
	VI	28	12	40
	EA	29	11	40
	Total	88	32	120

5 Conclusions

The results generated allowed to characterize in a quantitative way the effectiveness of IRT, VI and EA to detect soiling, partial shading and electrical faults, being 78%, 70% and 73% respectively. Statistical analysis determined that these differences do not mean that one technique is generally more effective than the others. However, analyzing each type of failure, significant differences were found

for the VI. This was the best technique detecting soiling (100%) in comparison to IRT (55%) and EA (60%), but it did not manage to detect any electric failure. In addition, partial shadows were the type of fault that was mostly detected by all the techniques, finding that none of the techniques is more effective than the others for this failure.

When comparing these results with those found in the research done by Cardinale-Villalobos (2020), it is identified that the calculated effectiveness depends on the design of the experiment, therefore, the protocols of each technique, the criteria for detection of failures and the treatments to be evaluated, must be carefully selected and documented in detail to support the results found.

The determination of the effectiveness of EA detecting soiling showed that the same treatment can be detected in some cases and not in others, therefore, this type of failure can be analyzed in more detail using this methodology increasing the replication of the treatments to increase the statistical power.

The results generated in this research, being of a quantitative nature, provide objective indicators that can be used by the managers of photovoltaic installations in the choice of the most convenient failure detection method for each need, contributing to mitigate a knowledge gap that has been detected in this area. In addition, it contributes to improve failure detection techniques, since information related to the strengths and limitations of each one is obtained. Finally, it will contribute to Sustainable Development due to the greater optimization of this renewable energy.

Acknowledgement

References

[Acciani et al., 2010] Acciani, G., Falcone, O., and Vergura, S. (2010). Typical defects of PV-cells. *IEEE International Symposium on Industrial Electronics*, pages 2745–2749.

[Appiah et al., 2019] Appiah, A. Y., Zhang, X., Ayawli, B. B. K., and Kyeremeh, F. (2019). Review and performance evaluation of photovoltaic array fault detection and diagnosis techniques. *International Journal of Photoenergy*, 2019:1–19.

[Bolboacă et al., 2011] Bolboacă, S. D., Jäntschi, L., Sestraş, A. F., Sestraş, R. E., and Pamfil, D. C. (2011). Pearson-fisher chi-square statistic revisited. *Information*, 2(3):528–545.

[Cardinale-Villalobos et al., 2020a] Cardinale-Villalobos, L., Meza, C., and Murillo-Soto, L. D. (2020a). Experimental comparison of visual inspection and infrared thermography for the detection of soling and partial shading in photovoltaic arrays. In Nesmachnow, S. and Hernández Callejo, L., editors, *Smart Cities, Third Ibero-American Congress, ICSC-Cities 2020, San José, Costa Rica, November 9-11, 2020, Revised Selected Papers*. Springer International Publishing, 1 edition.

[Cardinale-Villalobos et al., 2020b] Cardinale-Villalobos, L., Rimolo-Donadio, R., and Meza, C. (2020b). Solar panel failure detection by infrared uas digital photogrammetry: A case study. *International Journal of Renewable Energy Research (IJRER)*, 10(3):1154–1164.

[Chaudhary et al., 2018] Chaudhary, A. S., , and Chaturvedi, D. (2018). Analyzing defects of solar panels under natural atmospheric conditions with thermal image processing. *International Journal of Image, Graphics and Signal Processing*, 10(6):10–21.

[Flir, 2019] Flir (2019). Flir Vue Pro and Flir Vue Pro R.

[Flir.com, 2019] Flir.com (2019). Adjusting Sensitivity & Gain On The FLIR Vue Pro R.

[Gutiérreza-Pulido and De la Vara-Salazar, 2008] Gutiérreza-Pulido, H. and De la Vara-Salazar, R. (2008). *Análisis y diseño de experimentos*. McGraw-Hill Interamericana, México D.F, second edition.

[International Energy Agency, 2014] International Energy Agency (2014). Review of Failures of Photovoltaic Modules. Technical Report July, Performance and Reliability of Photovoltaic Systems.

[International Energy Agency, 2018] International Energy Agency (2018). Review on Infrared and Electroluminescence Imaging for PV Field Applications. Technical report, PHOTOVOLTAIC POWER SYSTEMS PROGRAMME.

[Javed et al., 2017] Javed, W., Wubulikasimu, Y., Figgis, B., and Guo, B. (2017). Characterization of dust accumulated on photovoltaic panels in doha, qatar. *Solar Energy*, 142:123–135.

[Jones and Schropp, 2000] Jones, J. B. and Schropp, M. A. (2000). Research fundamentals: Statistical considerations in research design: A simple person's approach. *Academic Emergency Medicine*, 7(2):194–199.

[Madeti and Singh, 2017] Madeti, S. R. and Singh, S. (2017). A comprehensive study on different types of faults and detection techniques for solar photovoltaic system. *Solar Energy*, 158:161–185.

[Maghami et al., 2016] Maghami, M. R., Hizam, H., Gomes, C., Radzi, M. A., Rezadad, M. I., and Hajighorbani, S. (2016). Power loss due to soiling on solar panel: A review. *Renewable and Sustainable Energy Reviews*, 59:1307–1316.

[Mchugh, 2009] Mchugh, M. L. (2009). The odds ratio: calculation, usage, and interpretation. *Biochemia medica*, 19(2):120–126.

[Mekki et al., 2016] Mekki, H., Mellit, A., and Salhi, H. (2016). Artificial neural network-based modelling and fault detection of partial shaded photovoltaic modules. *Simulation Modelling Practice and Theory*, 67:1–13.

[Mellit et al., 2018] Mellit, A., Tina, G., and Kalogirou, S. (2018). Fault detection and diagnosis methods for photovoltaic systems: A review. *Renewable and Sustainable Energy Reviews*, 91:1–17.

[Moretón et al., 2015] Moretón, R., Lorenzo, E., and Narvarte, L. (2015). Experimental observations on hot-spots and derived acceptance/rejection criteria. *Solar Energy*, 118:28–40.

[Murillo-Soto and Meza, 2020] Murillo-Soto, L. and Meza, C. (2020). Fault detection in solar arrays based on an efficiency threshold. In *2020 IEEE 11th Latin American Symposium on Circuits Systems (LASCAS)*, pages 1–4.

[Murillo-Soto and Meza, 2020] Murillo-Soto, L. D. and Meza, C. (2020). Diagnose algorithm and fault characterization for photovoltaic arrays: A simulation study. In *Lecture Notes in Electrical Engineering*, pages 567–582. Springer International Publishing.

[Mäki and Valkealahti, 2012] Mäki, A. and Valkealahti, S. (2012). Power losses in long string and parallel-connected short strings of series-connected silicon-based photovoltaic modules due to partial shading conditions. *IEEE Transactions on Energy Conversion*, 27(1):173–183.

[National Renewable Energy Laboratory, 2012] National Renewable Energy Laboratory (2012). Development of a Visual Inspection Data Collection Tool for Evaluation of Fielded PV Module Condition.

[Pradhan and Panda, 2020] Pradhan, R. and Panda, A. (2020). Performance evaluation of a MPPT controller with model predictive control for a photovoltaic system. *International Journal of Electronics*, 107(10):1543–1558.

[Tango, 2017] Tango, T. (2017). *Repeated Measures Design with Generalized Linear Mixed Models for Randomized Controlled Trials*. Taylor & Francis Group, Tokyo Japan.

[Tsanakas et al., 2016] Tsanakas, J. A., Ha, L., and Buerhop, C. (2016). Faults and infrared thermographic diagnosis in operating c-si photovoltaic modules: A review of research and future challenges. *Renewable and Sustainable Energy Reviews*, 62:695–709.

[Ventura-León, 2017] Ventura-León, J. L. (2017). El significado de la significancia estadística: comentarios a Martínez-Ferrer y colaboradores. *Salud Pública de México*, 59(5, sep-oct):499.

[Wang et al., 2016] Wang, Y., Itako, K., Kudoh, T., Koh, K., and Ge, Q. (2016). Voltage-based hot-spot detection method for defective cell in photovoltaic module using projector. *Journal of Energy and Power Engineering*, 10(8).

[Zefri et al., 2018] Zefri, Y., ElKettani, A., Sebari, I., and Lamallam, S. A. (2018). Thermal infrared and visual inspection of photovoltaic installations by UAV photogrammetry—application case: Morocco. *Drones*, 2(4):41.

[Zhao, 2015] Zhao, Y. (2015). Fault Detection, Classification and Protection in Solar Photovoltaic Arrays. Technical Report August, Massachusetts.

[Zhao et al., 2013] Zhao, Y., Lehman, B., Ball, R., Mosesian, J., and de Palma, J.-F. (2013). Outlier detection rules for fault detection in solar photovoltaic arrays. In *2013 Twenty-Eighth Annual {IEEE} Applied Power Electronics Conference and Exposition ({APEC})*. IEEE.

General discussion

To define the protocols of the failure detection techniques, the consulted literature shows that there is not a unique protocol, but one must be adapted for each particular case, for example, the IRT protocol depends on the characteristics of the camera, the drone, and the available software; in the case of the EA, it depends on the characteristics of the installation, the instrumentation and the model itself. These factors can have an impact on the results of each technique, due to the accuracy of the instrumentation. Therefore, the definition of the protocols for the implementation of each technique should be subjected to a rigorous analysis that should be adapted to each particular case. Also, it is convenient to make a cost analysis that allows finding the technique(s) that fit the available resources.

The protocols tested show that, for the results produced by each technique to be reliable, specific requirements must be met, even ensuring that certain environmental conditions exist. Such is the case of IRT, which may not be able to be used at a given moment due to a sudden decrease in irradiation. Therefore, to choose the most convenient failure detection method for a particular facility, protocols must be reviewed in detail to verify that it is possible to implement it on site.

The literature showed that some techniques have quantitative and other qualitative criteria for the detection of failures, for example, the VI in its traditional application uses only qualitative criteria, which makes the technique subject to subjectivity. On the other hand, the quantitative criteria of IRT and EA in some cases do not distinguish according to the type of failure and do not make a distinction in the severity, this implies that failures that are close to the failure threshold can be discharged or accepted; aspect like these caused that the effectiveness detecting soiling was lower than 60% for IRT and EA. The aspects indicated suggest that work should be done in the creation of quantitative criteria for the VI and better quantitative criteria for the IRT and EA for each type of failure and not in a general way.

The mentioned aspects allow detecting that, for future quantitative studies of failure detection techniques, the process of generation of each protocol and the criteria of failure detection used must be documented in detail, this way the results obtained will be supported and will contribute to the generation of better failure detection techniques.

The scientific literature of reference allowed generating the methodology to evaluate treatments that represented temporary failures, which, can continue being used to generate more experimental research with the possibility of not damaging the panels under test. The

methodology could be replicated taking the treatments used as a reference for a more detailed analysis of each type of failure, being the soiling the failure that was detected at a lower grade, therefore, more experimental research should be done around it. Including treatments of permanent failures and apparent failures (that do not have an impact on potency) will allow making a further characterization of the effectiveness of each failure detection method

The experiment results show that the effectiveness of the techniques evaluated depends on the types of failures evaluated and the number of treatments. For example, when comparing IRT and VI for soiling and partial shading failures, it was found that VI is more effective than IRT; however, when comparing the three techniques for the three types of failures, no technique was found to be more effective than the others. Therefore, future research of this type should include an analysis for each specific type of failure and include a characterization of the treatments evaluated.

It was found that the effectiveness calculated for each technique depends on the type of failure and that none of the techniques had the greatest effectiveness for all the types of failures evaluated. This suggests that to detect the greatest number of failures in a PV installation, it is not enough to use only one technique, but rather, combinations of techniques must be made. Since VI was the most effective at detecting soiling and IRT and EA were the most effective at detecting electrical faults, VI should be combined with IRT or EA to achieve the highest number of detected faults in a PV installation. Knowing the possible combinations of techniques to maximize failure detection, it is possible to continue with an economic analysis to choose the techniques to be used.

The results obtained represent the behavior of the techniques in similar installations and can be taken as a reference for use in photovoltaic systems with other characteristics. The replication and adaptation of this methodology in PV installations with another type of configuration (different numbers of panels and with parallel panel strings) is a task that must be done to continue the search for effectivity indicators that can be used in solar farms with a variety of configurations.

Global conclusions

Based on this research, through the specific protocols used and the experiment developed in the PV installation under test, the following conclusions were obtained:

1. The VI showed to be the most appropriate technique to detect soiling with effectiveness of 100%, while the IRT and EA had an effectiveness of 55% and 60% respectively.
2. IRT and EA proved to be the best techniques for detecting electrical faults, with effectivity of 100% and 83% respectively, while VI did not detect any electrical fault.
3. The effectivity of all the techniques detecting partial shadows was higher than 80%. Statistically, all techniques were found to be equally capable detecting this type of failure.
4. The overall effectiveness found for IRT, VI and EA was 78%, 70% and 73%. Through hypothesis testing with Fisher's exact test, this indicated that this does not represent a significant difference, that is, none of the techniques can be categorized in general terms as better than the others.
5. Regarding IRT, using quantitative criteria it was possible to detect failures objectively, however, 45% of the failures due to soiling were not detected. In these cases, the qualitative analysis allowed the identification of an apparent failure. This suggests that for this technique it is possible to establish new quantitative criteria for soiling.
6. To detect as many faults as possible, VI should be combined with IRT or EA; using a single technique, some faults will remain undetected.
7. It was proved that it is possible to analyze other failures and other techniques taking as reference the methodology used in this research, which allows validating models of failure detection techniques that have not been yet validated or compared empirically. For this, it is necessary to make an exhaustive analysis of the literature to define the suitable protocols for each technique and each type of failure of interest. Besides, the design of the experiment is a stage that must be focused on obtaining impartial results, where the resources to generate the treatments and quantity of experimental units to be used become a critical aspect to consider.
8. Quantitative indicators were determined based on empirical research, contributing to solve the problem of the lack of this information for the detection of faults in PV systems. Furthermore, they allow an objective and informed choice to be made about the type of technique to be used according to the type of failure that is considered most relevant to detect in a PV installation. Therefore, a contribution to sustainable development with more profitable PV systems is achieved over time.

Recommendations

1. To do more experimental research related to the detection of soiling through IRT and EA, focused on the generation of new criteria that increase the effectivity of detecting this type of failure.
2. To continue with the determination of the effectiveness of the techniques of failure detection, including experimentation with a greater number of treatments, so that it is possible to measure the capacity of each technique to differentiate between true positives and false positives. For this, treatments that do not generate a significant effect on potency, but are apparent failures, should be included.
3. To improve the EA method used through more empirical research that allows improving the mathematical model, adapting it to the particularities of the PV array and the accuracy of the instrumentation used.
4. To automate the detection of the failures of the techniques studied in this research, so that the subjectivity that could exist from a manual analysis is eliminated.

References

ACESOLAR. (2019). *Asociación costarricense de energía solar*. http://www.acesolar.org/que-es-generacion-distribuida/

Ali, Mohammed Hassan, Rabhi, Abdelhamid, Hajjaji, Ahmed El, Tina, G. M. (2016). Real Time Fault Detection in Photovoltaic Systems. *Energy Procedia*, *111*, 914–923.

Alsafasfeh, M., Abdel-Qader, I., & Bazuin, B. (2017, May). Fault detection in photovoltaic system using {SLIC} and thermal images. *2017 8th International Conference on Information Technology ({ICIT})*. https://doi.org/10.1109/icitech.2017.8079925

Appiah, A. Y., Zhang, X., Ayawli, B. B. K., & Kyeremeh, F. (2019). Review and Performance Evaluation of Photovoltaic Array Fault Detection and Diagnosis Techniques. *International Journal of Photoenergy*. https://doi.org/10.1155/2019/6953530

Asamblea General de las Naciones Unidas. (2019). *Naciones Unidas*. https://www.un.org/es/ga/president/65/issues/sustdev.shtml

Avendaño, M. (2017, November 11). *La utopía de una Costa Rica carbono neutral en 2021*. https://www.elfinancierocr.com/economia-y-politica/la-utopia-de-una-costa-rica-carbono-neutral-en/IYM5MH2PNZCP7BOHSZ5NV7CAQM/story/

Chaudhary, A. S., & and D.K. Chaturvedi. (2018). Analyzing Defects of Solar Panels under Natural Atmospheric Conditions with Thermal Image Processing. *International Journal of Image, Graphics and Signal Processing*, *10*(6), 10–21. https://doi.org/10.5815/ijigsp.2018.06.02

Chen, Y H, Liang, R, Tian, Y, Wang, F. (2016). A novel fault diagnosis method of PV based-on power loss and I-V characteristics. *Earth and Environmental Science*, *40*. https://doi.org/10.1088/1755-1315/40/1/012022

Chine, W., Mellit, A., Lughi, V., Malek, A., Sulligoi, G., & Pavan, A. M. (2016). A novel fault diagnosis technique for photovoltaic systems based on artificial neural networks. *Renewable Energy*, *90*, 501–512. https://doi.org/10.1016/j.renene.2016.01.036

Evans, D. L. (1981). Simplified method for predicting photovoltaic array output. *Solar Energy*, *27*(6), 555–560. https://doi.org/10.1016/0038-092X(81)90051-7

Gallardo-Saavedra, S., Hernández-Callejo, L., & Duque-Pérez, O. (2019). Quantitative failure rates and modes analysis in photovoltaic plants. *Energy*, *183*, 825–836. https://doi.org/10.1016/j.energy.2019.06.185

Grimaccia, F, Aghaei, M, Mussetta, M, Leva, S, Bellezza Quater, P. (2015). Planning for PV plant performance monitoring by means of unmanned aerial systems (UAS). *International Journal*

of Energy and Environmental Engineering, *6*(1), 47–54. https://doi.org/10.1007/s40095-014-0149-6

Gutiérrez Espeleta, Edgar E. (2015). *Plan Nacional de Energía 2015-2030*. https://minae.go.cr/recursos/2015/pdf/VII-PNE.pdf

Haney, J., & Burstein, A. (2013). *PV System operations and maintenance fundamentals.* www.solarabcs.org

Hernández Sampieri, R., Fernández Collado, C., Baptista, L., & Del Pilar, M. (2010). *Metodología de la investigación* (Fifth). Mc Graw Hill.

Herrera Murillo, J. (2017). *Estado de la Nación en Desarrollo Humano Sostenible 2017*. https://estadonacion.or.cr/files/biblioteca_virtual/023/Ambientales/Herrera_J_2017b.pdf

International Renewable Energy Agency. (2017). *Renewable*. https://www.irena.org/-/media/Files/IRENA/Agency/Publication/2018/Jan/IRENA_2017_Power_Costs_2018.pdf

Javed, W., Wubulikasimu, Y., Figgis, B., & Guo, B. (2017). Characterization of dust accumulated on photovoltaic panels in Doha, Qatar. *Solar Energy*, *142*, 123–135. https://doi.org/10.1016/j.solener.2016.11.053

Jones, C. B., Martinez-Ramon, M., Smith, R., Carmignani, C. K., Lavrova, O., Robinson, C., & Stein, J. S. (2016). Automatic fault classification of photovoltaic strings based on an in situ IV characterization system and a Gaussian process algorithm. *2016 IEEE 43rd Photovoltaic Specialists Conference (PVSC)*, 1708–1713. https://doi.org/10.1109/PVSC.2016.7749915

Kaplani, E. (2012). Detection of Degradation Effects in Field-Aged c-Si Solar Cells through IR Thermography and Digital Image Processing. *International Journal of Photoenergy*, *2012*, 11. https://doi.org/10.1155/2012/396792

Kazem, H. A., & Jabar H, Y. (2016). Modelling of Daily Solar Energy System Prediction using Support Vector Machine for Oman. *International Journal of Applied Engineering Research*, *11*, 10166–10172.

Land Instruments International. (2004). *A basic guide to thermography*. http://www.lirkorea.com/Landinstruments.net Website/infrared/downloads/pdf/thermography_guide.pdf

Livera, A., Theristis, M., Makrides, G., & Georghiou, G. E. (2019). Recent advances in failure diagnosis techniques based on performance data analysis for grid-connected photovoltaic systems. *Renewable Energy*, *133*, 126–143. https://doi.org/10.1016/j.renene.2018.09.101

Madeti, S. R., & Singh, S. N. (2017). A comprehensive study on different types of faults and detection techniques for solar photovoltaic system. *Solar Energy*, *158*, 161–185. https://doi.org/10.1016/j.solener.2017.08.069

Maghami, M. R., Hizam, H., Gomes, C., Radzi, M. A., Rezadad, M. I., & Hajighorbani, S. (2016). Power loss due to soiling on solar panel: A review. *Renewable and Sustainable Energy Reviews*, *59*, 1307–1316. https://doi.org/10.1016/j.rser.2016.01.044

Mäki, A., & Valkealahti, S. (2012). Power Losses in Long String and Parallel-Connected Short Strings of Series-Connected Silicon-Based Photovoltaic Modules Due to Partial Shading Conditions. *{IEEE} Transactions on Energy Conversion*, *27*(1), 173–183. https://doi.org/10.1109/tec.2011.2175928

María Fernanda, D. D. S. G., & Pérez-Ruiz. (2017). Análisis prospectivo del uso de energía solar: Caso Colombia. *Investigación y Ciencia: De La Universidad Autónoma de Aguascalientes*, *71*, 85–93.

Mata Jiménez, G. (2019, April 26). Nuevo Complejo Solar producirá del 25 al 30% de la energía eléctrica del Campus Tecnológico Central. *HOY EN EL TEC*. https://www.tec.ac.cr/hoyeneltec/2019/04/26/nuevo-complejo-solar-producira-25-30-energia-electrica-campus-tecnologico-central

McFarland, A. (2019). *U.S Energy Information Administration*. https://www.eia.gov/todayinenergy/detail.php?id=39092

Mekki, H., Mellit, A., & Salhi, H. (2016). Artificial neural network-based modelling and fault detection of partial shaded photovoltaic modules. *Simulation Modelling Practice and Theory*, *67*, 1–13. https://doi.org/10.1016/j.simpat.2016.05.005

Mellit, A., Chine, W., Massi Pavan, A., & Lughi, V. (2015). Fault diagnosis in photovoltaic arrays. *2015 International Conference on Clean Power (ICCEP)*. https://doi.org/10.1109/ICCEP.2015.7177602

Mellit, A., Tina, G. M., & Kalogirou, S. A. (2018). Fault detection and diagnosis methods for photovoltaic systems: A review. *Renewable & Sustainable Energy Reviews*, *91*, 1–17. https://doi.org/10.1016/j.rser.2018.03.062

Miguel A, R. J. . L., & Williams. (2016). Energía Solar. Serie de publicaciones científicas. *ACADEMIA NACIONAL DE CIENCIAS EXACTAS, FÍSICAS Y NATURALES*, *3*(10).

Moretón, R., Lorenzo, E., & Narvarte, L. (2015). Experimental observations on hot-spots and derived acceptance/rejection criteria. *Solar Energy*, *118*, 28–40. https://doi.org/10.1016/j.solener.2015.05.009

Murillo-Soto, L. D., & Meza, C. (2020a). Diagnose Algorithm and Fault Characterization for Photovoltaic Arrays: A Simulation Study. In *Lecture Notes in Electrical Engineering* (pp. 567–582). Springer International Publishing. https://doi.org/10.1007/978-3-030-37161-6_43

Murillo-Soto, L. D., & Meza, C. (2020b). Fault detection in solar arrays based on an efficiency

threshold. *2020 IEEE 11th Latin American Symposium on Circuits and Systems, LASCAS 2020*. https://doi.org/10.1109/LASCAS45839.2020.9069046

National renewable energy laboratory. (2012). Development of a Visual Inspection Data Collection Tool for Evaluation of Fielded PV Module Condition. In *NREL Technical Report* (Issue August). https://doi.org/10.2172/1050110

Nemet, Gregory F, O'Shaughnessy, Eric, Wiser, Ryan, Darghouth, N. (2017). Characteristics of low-priced solar PV systems in the U.S. *Applied Energy*, *187*, 501–513. https://doi.org/10.1016/j.apenergy.2016.11.056

Palmer Wahl Instrumentation group. (2007). *The evolution of thermal imaging cameras*. http://instrumentation.com/PDFS/EvolutionThermalImagingCameras.pdf

Rolf Frischknecht, René Itten, Parikhit Sinha, Mariska de Wild-Scholten, Jia Zhang. (2015). *Life Cycle Inventories and Life Cycle Assessments of Photovoltaic Systems*. http://www.iea-pvps.org/fileadmin/dam/public/report/technical/IEA-PVPS_Task_12_LCI_LCA.pdf

Tango, T. (2017). *Repeated Measures Design with Generalized Linear Mixed Models for Randomized Controlled Trials* (S.-C. Chow (ed.)). Taylor & Francis Group.

Tecnológico de Costa Rica. (2017). *Plan Estratégico 2017-2021*. https://www.tec.ac.cr/sites/default/files/media/doc/plan_estrategico_2017_0.pdf

Tsanakas, J. A., Ha, L., & Buerhop, C. (2016). Faults and infrared thermographic diagnosis in operating c-Si photovoltaic modules: A review of research and future challenges. *Renewable and Sustainable Energy Reviews*, *62*, 695–709. https://doi.org/10.1016/j.rser.2016.04.079

United Nations. (2015). The Millennium Development Goals Report. In *United Nations*. https://www.undp.org/content/dam/undp/library/MDG/english/UNDP_MDG_Report_2015.pdf

Ventura, C., & Tina, G. M. (2016). Utility scale photovoltaic plant indices and models for on-line monitoring and fault detection purposes. *Electric Power Systems Research*, *136*, 43–56. https://doi.org/10.1016/j.epsr.2016.02.006

Watson, J. J. W., & Hudson, M. D. (2015). Regional Scale wind farm and solar farm suitability assessment using {GIS}-assisted multi-criteria evaluation. *Landscape and Urban Planning*, *138*, 20–31. https://doi.org/10.1016/j.landurbplan.2015.02.001

Wohlin, C., Runeson, P., Höst, M., Ohlsson, M. C., Regnell, B., & Wesslén, A. (2012). *Experimentation in Software Engineering*. Springer Berlin Heidelberg. https://doi.org/10.1007/978-3-642-29044-2

Yadong Wang, Kazutaka Itako, Tsugutomo Kudoh, Keishin Koh, & Qiang Ge. (2016). Voltage-Based Hot-Spot Detection Method for Defective Cell in Photovoltaic Module Using Projector.

Journal of Energy and Power Engineering, *10*(8). https://doi.org/10.17265/1934-8975/2016.08.005

Zhao, Y. (2015). *Fault Detection, Classification and Protection in Solar Photovoltaic Arrays* (Issue August). http://hdl.handle.net/2047/D20195700

Annexes

Annex A. General technical characteristics of the instrumentation

Irradiance sensor

Brand: TRITEC

Model: Spektron 2010

Voltage output: 77.23 mV at 1000 W/m2

Accuracy: ± 5% of the annual average

Construction: Laminated in Novaflon and EVA film.

Degree of protection: IP65

Dimensions: 118mm / 50 mm / 44 mm.

Fig 8. Photograph of the Spektron 2010 irradiance sensor used. Source: Manufacturer's sheet.

Power measurement

Equipment: Inverter

Brand: SMA.

Model: SUNNY BOY 3.8-US

Comunication: Ethernet.

Accuracy: According to ANSI C12.20 standard, they can be used for billing

Measurement of ambient temperature

Equipment: Weather station

Brand: DAVIS

Weather station model: Vantage Pro2

Temperature sensor: Silicon junction diode PN

Accuracy: 0.3 °C

Cell temperature measurement

Equipment: Contact temperature sensor.

Brand: GAIMC

Model DS18B20

Measurement format: Digital

Accuracy: ± 0.5 °C

Annex B. Geographical location of the site under study

The TEC's PV installation is distributed between the technology campuses of Cartago and San Carlos (see Fig 9). The geographical distribution of the equipment of interest in this study is shown in Fig 10.

Fig 9. Location of Central Technological Campus (Campus Central) and San Carlos Local Technological Campus (SC Campus). The experiment of this research was made in the SC Campus. Image taken from Google Earth.

Fig 10. Aerial photograph with the location of the parts of the PV installation in San Carlos. The PV strings are enclosed in a red box. Image taken and adapted from Google Earth.

Annex C. Technical characteristics of the PV modules

Electrical characteristics of the PV module used

ELECTRICAL DATA / STC*

CS6K	275M	280M	285M
Nominal Max. Power (Pmax)	275 W	280 W	285 W
Opt. Operating Voltage (Vmp)	31.3 V	31.5 V	31.7 V
Opt. Operating Current (Imp)	8.80 A	8.89 A	8.98 A
Open Circuit Voltage (Voc)	38.3 V	38.5 V	38.6 V
Short Circuit Current (Isc)	9.31 A	9.43 A	9.51 A
Module Efficiency	16.80 %	17.11 %	17.41 %
Operating Temperature	-40°C ~ +85°C		
Max. System Voltage	1000 V (IEC) or 1000 V (UL)		
Module Fire Performance	TYPE 1 (UL 1703) or CLASS C (IEC 61730)		
Max. Series Fuse Rating	15 A		
Application Classification	Class A		
Power Tolerance	0 ~ + 5 W		

* Under Standard Test Conditions (STC) of irradiance of 1000 W/m², spectrum AM 1.5 and cell temperature of 25°C.

ELECTRICAL DATA / NOCT*

Electrical Data CS6K	275M	280M	285M
Nominal Max. Power (Pmax)	199 W	202 W	206 W
Opt. Operating Voltage (Vmp)	28.5 V	28.7 V	28.9 V
Opt. Operating Current (Imp)	6.95 A	7.04 A	7.12 A
Open Circuit Voltage (Voc)	35.1 V	35.3 V	35.4 V
Short Circuit Current (Isc)	7.54 A	7.63 A	7.70 A

* Under Nominal Operating Cell Temperature (NOCT), irradiance of 800 W/m², spectrum AM 1.5, ambient temperature 20°C, wind speed 1 m/s.

Mechanical characteristics of the PV module used

MECHANICAL DATA

Specification	Data
Cell Type	Mono-crystalline, 6 inch
Cell Arrangement	60 (6×10)
Dimensions	1650×992×40 mm (65.0×39.1×1.57 in)
Weight	18.2 kg (40.1 lbs)
Front Cover	3.2 mm tempered glass
Frame Material	Anodized aluminium alloy
J-Box	IP67, 3 diodes
Cable	4 mm² (IEC) or 4 mm² & 12 AWG 1000 V (UL), 1000 mm (39.4 in)
Per Pallet	26 pieces, 520 kg (1146.4 lbs) (quantity & weight per pallet)
Per container (40' HQ)	728 pieces

Thermal characteristics of the PV module used

TEMPERATURE CHARACTERISTICS

Specification	Data
Temperature Coefficient (Pmax)	-0.41 % / °C
Temperature Coefficient (Voc)	-0.31 % / °C
Temperature Coefficient (Isc)	0.053 % / °C
Nominal Operating Cell Temperature	45±2 °C

Performance guaranteed by the manufacturer

THIRTY (30) YEAR
LIMITED PERFORMANCE WARRANTY

Canadian Solar guarantees that for a period of thirty years the module will maintain a performance as set forth

below:

- During the first year, Canadian Solar guarantees the actual power output of the module will be no less than 97.5% of the labeled power output.
- From year 2 to year 30, the actual annual power decline will be no more than 0.5 %; by the end of year 30, the actual power output will be no less than 83 % of the labeled power output.

Ageing loss calculation

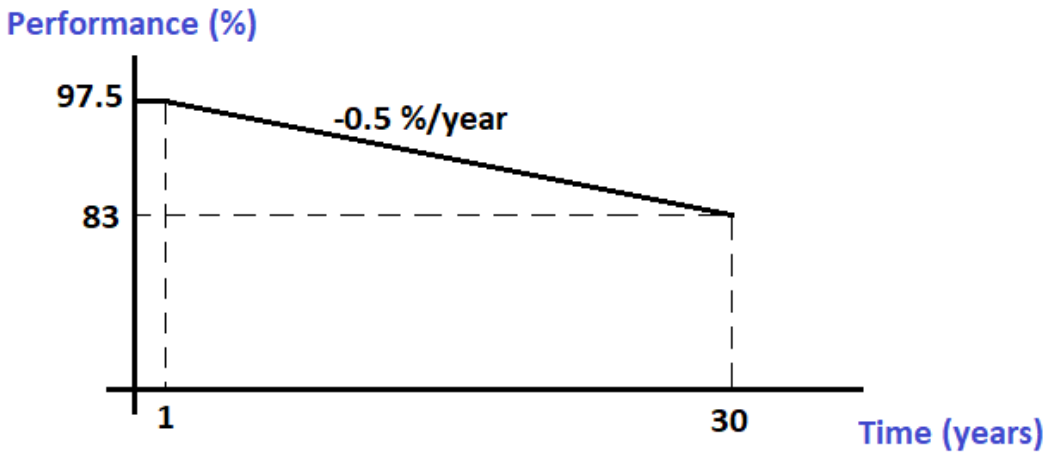

Considering the annual performance drop of 0.5 % from the second year and the minimum performance guaranteed by the manufacturer at the end of the first year, ageing losses are calculated with (5).

$$l_y = 0.005(\mathrm{t} - 1) + 0.025 \qquad (4)$$